Estimation of chromophoric dissolved organic matter in the Mississippi and Atchafalaya river plume regions using above-surface hyperspectral remote sensing

Weining Zhu,[1] Qian Yu,[1] Yong Q. Tian,[2] Robert F. Chen,[2] and G. Bernard Gardner[2]

Received 14 July 2010; revised 14 October 2010; accepted 29 November 2010; published 9 February 2011.

[1] A method for the inversion of hyperspectral remote sensing was developed to determine the absorption coefficient for chromophoric dissolved organic matter (CDOM) in the Mississippi and Atchafalaya river plume regions and the northern Gulf of Mexico, where water types vary from Case 1 to turbid Case 2. Above-surface hyperspectral remote sensing data were measured by a ship-mounted spectroradiometer and then used to estimate CDOM. Simultaneously, water absorption and attenuation coefficients, CDOM and chlorophyll fluorescence, turbidities, and other related water properties were also measured at very high resolution (0.5–2 m) using in situ, underwater, and flow-through (shipboard, pumped) optical sensors. We separate a_g, the absorption coefficient a of CDOM, from a_{dg} (a of CDOM and nonalgal particles) based on two absorption-backscattering relationships. The first is between a_d (a of nonalgal particles) and b_{bp} (total particulate backscattering coefficient), and the second is between a_p (a of total particles) and b_{bp}. These two relationships are referred as a_d-based and a_p-based methods, respectively. Consequently, based on Lee's quasi-analytical algorithm (QAA), we developed the so-called Extended Quasi-Analytical Algorithm (QAA-E) to decompose a_{dg}, using both a_d-based and a_p-based methods. The absorption-backscattering relationships and the QAA-E were tested using synthetic and in situ data from the International Ocean-Colour Coordinating Group (IOCCG) as well as our own field data. The results indicate the a_d-based method is relatively better than the a_p-based method. The accuracy of CDOM estimation is significantly improved by separating a_g from a_{dg} (R^2 = 0.81 and 0.65 for synthetic and in situ data, respectively). The sensitivities of the newly introduced coefficients were also analyzed to ensure QAA-E is robust.

Citation: Zhu, W., Q. Yu, Y. Q. Tian, R. F. Chen, and G. B. Gardner (2011), Estimation of chromophoric dissolved organic matter in the Mississippi and Atchafalaya river plume regions using above-surface hyperspectral remote sensing, *J. Geophys. Res.*, *116*, C02011, doi:10.1029/2010JC006523.

1. Introduction

[2] Dissolved organic carbon (DOC), the carbon content of dissolved organic matter (DOM), is one of the largest carbon pools in aquatic systems [*Amon and Benner*, 1994; *Carlson et al.*, 1994]. As the photoactive fraction of DOM, chromophoric dissolved organic matter (CDOM) in seawater can be used as a tracer of terrestrial DOC in the marine environment [*Blough et al.*, 1993; *Del Castillo et al.*, 1999; *Jerlov*, 1976]. Many observations provide evidence of a good correlation between CDOM and DOC loading across the different subcatchments [*Ferrari et al.*, 1996; *Kowalczuk et al.*, 2005b; *Mannino et al.*, 2008; *Stedmon et al.*, 2006; *Vodacek et al.*, 1997], despite the absence of this covariation in a few cases [*Chen et al.*, 2004]. Together with the other two ocean color components, chlorophyll and nonalgal particles (NAP), CDOM plays an important role in determining photochemical characteristics of water in nature; its high optical absorption at short wavelengths (350–440 nm) may affect the photosynthesis of aquatic phytoplankton [*Bukata et al.*, 1995; *Kirk*, 1994]. In addition, due to its biotic sources, CDOM is also a good proxy for monitoring the dynamics of organic ecosystems [*Doney et al.*, 1995; *Shooter and Brimblecombe*, 1989; *Valentine and Zepp*, 1993].

[3] Since CDOM has an effect on the underwater light field and water's inherent optical properties (IOP), and consequently determines the L_w (water-leaving radiance) or R_{rs} (remote sensing reflectance) received by above-surface remote sensors, inversion of remote sensing data provides a rapid and efficient approach to estimate CDOM within a large spatial-temporal scale [*Sathyendranath*, 2000; *Lee*, 2006; *Mobley*, 1994]. Hence in ocean color sciences, CDOM's absorption properties (e.g., its absorption coeffi-

[1]Department of Geosciences, University of Massachusetts Amherst, Amherst, Massachusetts, USA.
[2]Department of Environmental, Earth and Ocean Sciences, University of Massachusetts Boston, Boston, Massachusetts, USA.

0148-0227/11/2010JC006523

cients at 440 nm) are usually used as a proxy of its concentration [*Nelson and Siegel*, 2002]. In the earliest algorithms using CZCS (Coastal Zone Color Scanner), chlorophyll's concentrations were empirically inverted and CDOM can be accordingly assessed with the hypothesis that it covaries with chlorophyll [*Gordon and Morel*, 1983; *Hoge et al.*, 1995; *Morel and Prieur*, 1977]. Later, several semianalytical models have been developed and applied to SeaWiFS (Sea-viewing Wide Field-of-view Sensor) and MODIS (Moderate Resolution Imaging Spectroradiometer) [*Carder et al.*, 1999; *Garver and Siegel*, 1997; *O'Reilly et al.*, 1998; *Siegel et al.*, 2002], in which CDOM's absorption coefficients are directly and independently inverted from R_{rs}. The semianalytical models are based on the radiative transfer equations as well as the simplification of radiance and underwater light field [*Mobley*, 1994]. Recently, in situ hyperspectral measurements with newly developed remote sensing reflectance models [*Lee et al.*, 1999] have also been used to estimate CDOM as one of ocean color components, such as AVIRIS (Airborne Visible Infrared Imaging Spectrometer) with model-driven optimization [*Lee et al.*, 2001], and EO-1 Hyperion with MIM (Matrix Inversion Method) [*Brando and Dekker*, 2003]. These recent methods combine hyperspectral remote sensing data, some semianalytical models, new factors (e.g., the bottom effects) and computational techniques, and hence improve the accuracy of CDOM inversion.

[4] Among those semianalytical models, a bio-optical model is widely used—it is a simplified 3-component model that only takes account of three major constituents usually present in water: phytoplankton (mainly chlorophyll), CDOM, and detritus (or nonalgal particle, NAP). In this model, the water's absorption and backscattering coefficients, $a(\lambda)$ and $b_b(\lambda)$, are expressed as

$$a(\lambda) = a_w(\lambda) + a_{ph}(\lambda) + a_g(\lambda) + a_d(\lambda) \quad (1)$$

and

$$b_b(\lambda) = b_{bw}(\lambda) + b_{bp}(\lambda), \quad (2)$$

respectively, where the subscripts, *w*, *ph*, *g* and *d* denote the contributions of pure seawater, phytoplankton, CDOM, and NAP, respectively, and *p* in the backscattering term means the total particulate backscattering coefficients including both phytoplankton and NAP. For absorption coefficients, a_g and a_d are usually combined in one term, a_{dg}, so-called colored detrital matter (CDM) [*Siegel and Michaels*, 1996].

[5] Most previous CDOM inversion algorithms have derived a_{dg} rather than a_g. There are three major reasons for not separating a_g from a_{dg}. First, CDOM and NAP have similar spectral shapes and slopes [*Bricaud et al.*, 1981; *Kirk*, 1994]:

$$a_{d/g}(\lambda) = a_{d/g}(\lambda_{ref}) \exp\left(-S_{d/g}(\lambda - \lambda_{ref})\right), \quad (3)$$

where $a_{d/g}(\lambda)$ denotes $a_d(\lambda)$ or $a_g(\lambda)$, and $S_{d/g}$ denotes corresponding S_d or S_g. The reference wavelength λ_{ref} is chosen to be 440 nm or 443 nm, and the spectral slope $S_{d/g}$ often ranges from about 0.011 to 0.025 nm^{-1} [*Bricaud et al.*, 1981, 1998; *Carder et al.*, 1989; *Green and Blough*, 1994; *Kratzer et al.*, 2000; *Roesler et al.*, 1989; *Yentsch*, 1962]. Consequently, it is difficult to distinguish their absorptions from each other. Second, the previous research focused more on estimating a_{ph} due to the interests on phytoplankton pigments, particularly chlorophyll a [*O'Reilly et al.*, 1998; *Sathyendranath et al.*, 1994]. a_{dg} is more likely the by-product so that it is not necessary to separate it further. Third, the majority of ocean color algorithms are targeted and applied for Case 1 water in open seas, where CDOM and NAP were observed to covary well with the phytoplankton [*Morel and Prieur*, 1977; *Prieur and Sathyendranath*, 1981]. In addition, the fraction of NAP in Case 1 water is very low. For example, according to *Nelson et al.* [1998], NAP contributes only 9% of the nonwater absorption at 440 nm in the Sargasso Sea. As a result, a_d's contribution to a_{dg} is negligible.

[6] With increasing interests in CDOM, it is essential to decompose a_{dg} and derive a_g through an accurate inversion. More recent observations suggest that the CDOM-chlorophyll covariation are weak and controversial even for Case 1 water [*Carder et al.*, 1999], and may either overestimate or underestimate chlorophyll and hence CDOM [*Arrigo et al.*, 1994; *Hochman et al.*, 1994]. Many CDOM studies aim to trace and monitor the dynamics of terrigenous DOC and therefore pay more attention to inland, estuarine and coastal water, so-called Case 2 water. Case 2 water contains more CDOM derived from terrestrial vegetation than from the local in-water phytoplankton [*Nelson and Siegel*, 2002], and therefore CDOM and chlorophyll are generally independent. Moreover, high concentrations of NAP are often observed in Case 2 water, which have a considerable contribution to a_{dg} [*Sathyendranath*, 2000]. All these reasons indicate that separation of a_{dg} is necessary for Case 2 water and sometimes even for Case 1 water.

[7] Separating a_{dg} is a very challenging task and not well investigated. Several published algorithms are able to retrieve a_g and a_d separately, but their applications are limited for various reasons [*Lee*, 2006]. The empirical algorithms are difficult to extrapolate and may result in significant errors [*Kowalczuk et al.*, 2005a; *Lee et al.*, 1998; *Sathyendranath et al.*, 2001]. Forward optimizations and LUT (look-up table) methods are time consuming and hence unfavorable to handle large data sets, such as satellite images [*Lee et al.*, 1996; *Liu and Miller*, 2008; *Van Der Woerd and Pasterkamp*, 2008]. The accuracy of semianalytical algorithms, such as MIM, depends on the accurate preset of spectral models for each individual ocean color component [*Barnard et al.*, 1999; *D'Sa et al.*, 2006; *Doerffer and Fischer*, 1994; *Green et al.*, 2008; *Hoge and Lyon*, 1996]. Some of the pure statistical techniques, such as PCA (principal component analysis) and aNN (artificial neural network), lack analytical and theoretical bases, and the results might be hard to interpret [*Doerffer and Schiller*, 1998; *Fischer*, 1985; *Mueller et al.*, 2003; *Sandidge and Holyer*, 1998]. On the other hand, due to our insufficient knowledge of the interaction and dynamics of in-water photochemical constituents plus the extreme complexity of radiative transfer, a fully analytical inversion model is still unreachable [*Sathyendranath*, 2000; *Mobley*, 1994].

[8] The main objective of the present study is to develop a proper quasi-analytical approach to invert the exact CDOM absorption from above-surface remote sensing. To reach this goal, very high resolution measurements were conducted on

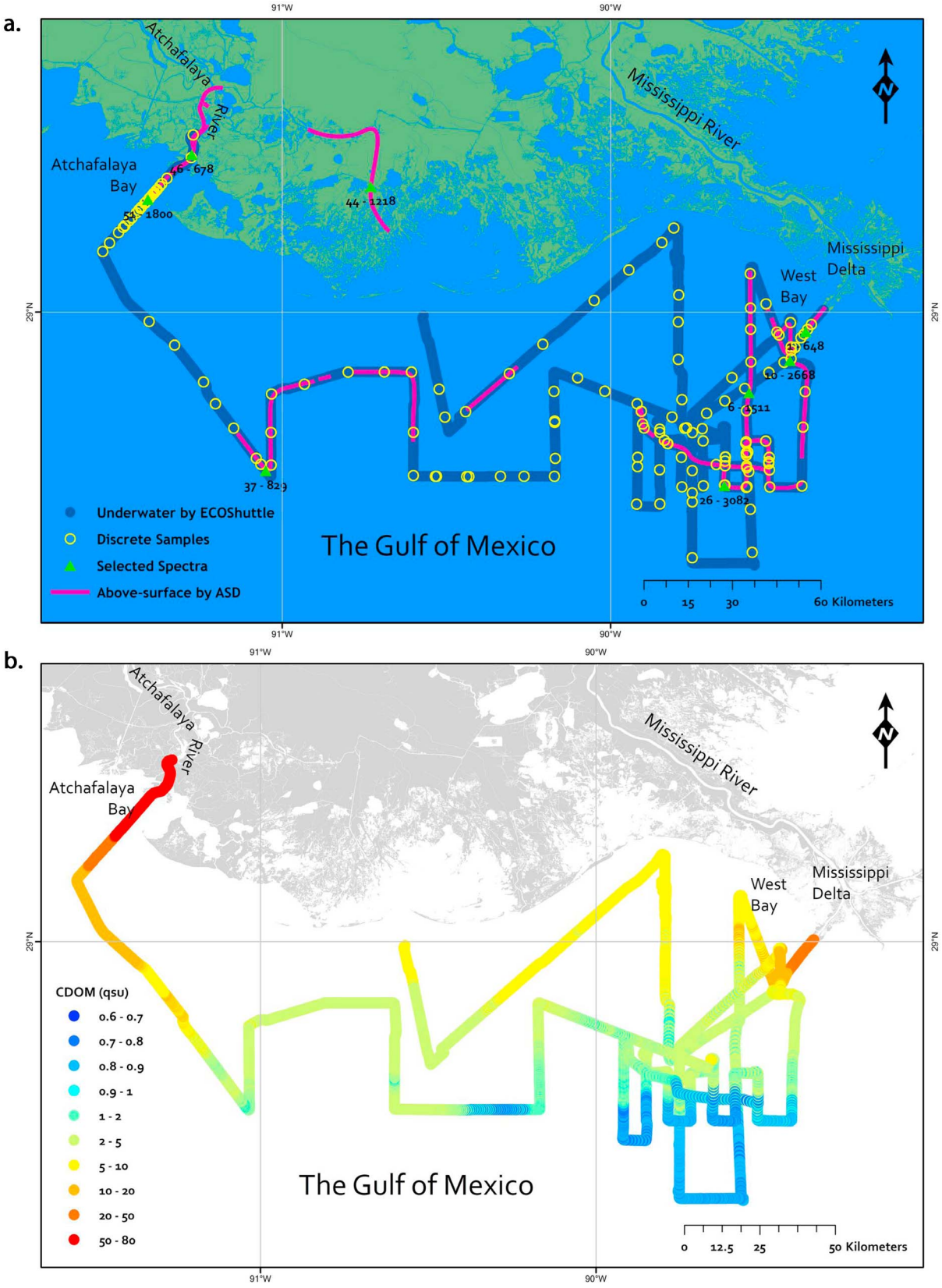

Figure 1. (a) Cruise tracks of above-surface (by ASD) and underwater (by ECOShuttle) measurements and discrete water sampling locations in the Mississippi and Atchafalaya river plumes and the northern Gulf of Mexico. The spectra and properties of 7 selected samples are shown in Figure 5 and Table 1, respectively. (b) Measured CDOM concentrations (QSU) along the tracks.

the Mississippi and Atchafalaya river plumes as well as the northern Gulf of Mexico, where CDOM, chlorophyll and NAP's variations are large and water types are diverse from simple Case 1 to complex Case 2. About 300,000 in situ measurements of CDOM, chlorophyll, NAP, water's IOPs and other properties, as well as 20,000 water hyperspectra were collected almost simultaneously, providing a huge data set for ocean color study. Based on the former quasi-analytical algorithm (QAA), we developed an extension to separate a_g from a_{dg}. The results show that the proposed separation method performs excellently and is promising for future satellite image inversion.

2. Data Acquisition

2.1. Study Site

[9] The Mississippi River is the longest river in the United States, and its watershed occupies about 41% of total continental area of the Unite States. At Old River Junction, a man-made system controls the flow of the Mississippi River to the Gulf of Mexico. The U.S. Army Corps of Engineers reports that seventy percent of the flow drains out of the Birdfoot region through the lower Mississippi River while thirty percent is diverted to the Atchafalaya basin, forming the Atchafalaya River [*U.S. Army Corps of Engineers*, 2008]. Both outlets in the Gulf of Mexico form large plumes containing high sediment and organic matter concentrations. The lower Atchafalaya River passes through wetlands, salt marshes and bayous, and empties into the shallow Atchafalaya Bay with a large capacity to trap sediment. Also, the near coastal wetlands are highly productive ecosystems which interact with riverine and estuarine waters and represent a source of coastal CDOM [*Lane et al.*, 2002; *Pakulski et al.*, 2000]. On the other hand, the lower Mississippi holds a catchment with low vegetation coverage that has been highly channelized. Therefore, the interaction of the river with historical floodplains is greatly reduced and is therefore expected to have lower CDOM inputs to the Gulf of Mexico than the Atchafalaya.

[10] The in situ CDOM concentration and spectral data were measured on the RV Pelican during a 7 day cruise, 23–29 August 2007, in the Mississippi and Atchafalaya river plume regions as well as the northern Gulf of Mexico. The cruise tracks were designed to cross the CDOM gradients in the plumes, aiming to capture the largest variations in CDOM. The data acquisition activities include (1) continuous above-surface hyperspectral measurements of water apparent optical properties (AOP), (2) continuous underwater measurements of temperature, salinity, density, dissolved oxygen and UV radiance, CDOM fluorescence, chlorophyll fluorescence, optical backscatter, and depth, (3) continuous measurements of the IOPs (absorption and backscattering coefficients) of water pumped from the sampling platform, and (4) discrete water sampling from the pumped water for analysis of absorption spectra, CDOM fluorescence, and dissolved organic carbon in the laboratory. The GPS-derived ship position was recorded concurrently with the in situ data. The site map, cruise track, and sampling locations of above measurements are illustrated in Figure 1a.

2.2. Above-Surface Hyperspectral Measurements

[11] The above-surface remote sensing reflectance of seawater was measured by a portable spectroradiometer (Applied Spectral Devices FieldSpec®3), with a full spectral range (350–2500 nm). The spectral sampling interval of output is 1 nm. The fiber optic collection sensor was mounted on the bow of the vessel pointed straight down at the sea surface at a height of approximately 4 m. The sensor was mounted in a way that the sensor could be turned by hand to measure water total radiance/reflectance (down), sky radiance (up), or at a white barium oxide white board (down) for calibration. The above-surface measurement was referred to NASA's ocean optics protocols for satellite ocean color sensor validation [*Mueller et al.*, 2003].

[12] The measurements were continuous during the daytime, from around 08:30 to 18:30 local time. Data were not collected during very high seas that created white caps. During the entire cruise, we collected 75 data sets with approximately 20,000 hyperspectral samples. Each data set contains 100 to 3000 samples that were obtained under similar illumination conditions with individual sky radiance measurements and white board calibrations. The calibration frequency between each data set depended on the change of solar zenith and illumination conditions throughout the day, particularly considering cloud and wind conditions, typically every 20–30 min or less. The frequency of sampling was approximately 5–20 s per sample depending on CDOM gradient and navigation speed (lower frequency for open sea and higher frequency for river plume regions). Each sample is an average of 10 spectral measures to reduce the noise [*Analytical Spectral Devices, Inc.*, 2009]. The weather during the cruise was in general sunny, occasionally with light clouds and gentle wind, except for a few hours of strong winds on 23 August. Sampling locations were recorded by a GPS unit synchronized with the Analytical Spectral Devices (ASD) spectroradiometer.

[13] Compared with the satellite images, the in situ above-surface hyperspectral measurements bear two advantages: (1) much less atmospheric effect and (2) better synchronization to the in situ CDOM measurements. One goal of our project is to investigate whether above-surface hyperspectral remote sensing is capable of estimating CDOM concentration in ocean and coastal waters with satisfactory accuracy. This knowledge will contribute to our ability to estimate coastal CDOM concentrations from hyperspectral satellite images such as those from EO-1 Hyperion.

2.3. Underwater Measurements

[14] In situ underwater measurements were carried out using the ECOShuttle, a towed, undulating vehicle based on the Nu-Shuttle manufactured by Chelsea Instruments. Instrumentation mounted inside the ECOShuttle include a SeaBird Electronics SBE 9/11 CTD system providing temperature, salinity and depth measurements; a CDOM fluorometer, a chlorophyll fluorometer and an optical backscatter sensor (OBS) manufactured by Seapoint Sensors, Inc; and a YSI dissolved oxygen sensor provided by SeaBird Electronics. The CTD is calibrated at the factory annually. CDOM voltages were compared with discrete samples and converted to quinine sulfate units (QSU) equivalent to 1 μg/l of quinine sulfate at pH = 2, λ_{ex} = 337 nm,

and λ_{em} = 450 nm. Chlorophyll fluorescence was calibrated using the factory suggested conversion factor. The ECOShuttle was generally programmed for a sawtooth pattern from 2–3 m depth (just below the influence of the ship's wake) to a depth 5 m above the bottom (to avoid the bottom). Ship speed was 6–8 knots. The sampling resolution was in the range of 0.5–2 m (around 3 samples per second) along the cruise track. About 1,000,000 underwater measurements were acquired. To minimize the random error, we averaged the successive measurements within every 0.2 m depth, which resulted in 300,000 measurements used in the study.

[15] In addition, a stainless steel well pump mounted on the underside of the ECOShuttle pumped uncontaminated (only touches stainless steel and Teflon) seawater into the shipboard lab via a 0.5-inch ID Teflon tube in the tow cable. This seawater flow was distributed into a Wetlabs AC-9 multispectral absorption meter that measures the water's total attenuation and absorption coefficients at 9 wavelengths (412, 440, 488, 510, 532, 555, 650, 676, 715 nm). Milli-Q water was used as a reference. In addition, the flowing seawater supplies a source for discrete sample analysis of DOC and optical properties. Complete details of the ECOShuttle system are given by *Chen* [1999], *Chen et al.* [2004], and *Chen and Gardner* [2004].

2.4. Discrete Samples

[16] Discrete water samples supplied by the ECOShuttle's pumping system were collected to calibrate the real time underway measurements (Figure 1a). The interval of sampling was generally determined by the ECOShuttle depth, the sampling lag time and the location. When a sample was to be taken, an instantaneous record of the in situ data was produced and a stopwatch started to determine the exact time for collection. Samples were drawn precisely after the determined delay time had passed (the ECOShuttle generally spent 10–20 s at the surface). The delay time was determined by matching salinity minima and maxima as the ECOShuttle undulated through a river plume, usually around 4 min. Careful alignment of in-line data with ECOShuttle data was made after the cruise. Fluorescence of filtered seawater samples was measured with a Photon Technologies International Quantum Master-1 spectrofluorometer equipped with a double excitation monochromator, a single emission monochromator and a cooled photomultiplier assembly. CDOM absorption spectra (200–800 nm) were measured by a Cary 50 spectrophotometer with a 1 cm path length cell. The details of lab processing and computation were described by *Huang and Chen* [2009].

3. Methods

3.1. Data Preprocessing

3.1.1. Above-Surface Hyperspectra

[17] The radiance received by the above-surface spectroradiometer includes both water-leaving radiance and the radiance from the water surface reflection. Water surface reflection contains no information about the in-water constituents, but contaminates the subsurface volumetric radiance. Before inversion, the surface radiance need to be removed to obtain the remote sensing reflectance or water-leaving radiance, which are the eligible inputs of inverse algorithms [*Yu et al.*, 2010].

[18] Remote sensing reflectance R_{rs} at given direction (θ, φ) and wavelength λ is calculated by *Mobley* [1999]

$$R_{rs} = \frac{R_g(L_t - L_r)}{\pi L_g}, \tag{4}$$

where L_t is the total water radiance received by sensors, and L_r is the radiance reflected by the sea surface. Hence $L_t - L_r$ is the water-leaving radiance; L_g is the radiance reflected by the Spectralon reference panel (white reference); and the R_g is the reflectance of the white reference. Since the white reference is a Lambertian surface, R_g is equivalent to irradiance reflectance, defined as the ratio of upward planar irradiance and downward planar irradiance. $\pi L_g/R_g$ gives the downwelling spectral plane irradiance incident onto the sea surface.

[19] In equation (4), technically we could not measure L_r directly but it can be approximately computed by $L_r \approx \rho L_s$, where L_s is sky radiance from the corresponding incident angle and the ρ is the ratio representing the proportion of L_r to L_s. In our cruise, we mainly recorded the total water reflectance R_t, instead of the L_t (only a small number of L_t were recorded for calibration purpose). In ASD, R_t is determined by $R_t = L_t/L_g$. Therefore equation (4) could be rewritten by all directly measured variables, except ρ, that is,

$$R_{rs} = \frac{R_g}{\pi}\left(R_t - \frac{\rho L_s}{L_g}\right). \tag{5}$$

R_g is in the range of 0.990 to 0.992 at wavelengths from 400 to 700 nm. ρ was simulated individually for each data set using Hydro-Ecolight® [*Mobley and Sundman*, 2008], with specific in situ solar zenith, wind speed, cloud cover, and other atmospheric properties. We used a nadir view, rather than the recommended viewing angles of zenith 45° and azimuth 135°. The reason is for a consecutive measurement along the cruise, this nadir viewing angle keeps fixed sensor-Sun geometry, and the sensor azimuth angle φ is independent of ship moving direction. Therefore the sensor view angle is consistent while the vessel frequently alters its navigating direction at varying time of day (different solar angle). In addition, according to the previous results [*Mobley*, 1999, Figure 7], the nadir view, that is, $\theta = 0°$ and $\varphi = 0°$, is beneficial in removing water surface reflectance. In our calculation, we found that ρ slightly varied with solar zenith and wind speed, but was highly impacted by cloud cover. For solar zenith $\theta > 30°$, wind speed < 5 m/s and clear sky, ρ for the nadir viewing is approximately 0.021. The spectral data measured with solar zenith $\theta < 20°$ (around 11:30 A.M.–12:30 P.M.), wind speed > 10 m/s, or under cloud shadow were not included in the analysis due to the induced high uncertainty.

3.1.2. CDOM Concentration and Water's IOP

[20] Due to complex and variable CDOM chemistry, CDOM concentration is usually represented by its optical properties, for example, the fluorescence intensity, rather than its physical mass, as the mg/l or g/l used for chlorophyll and NAP. In ocean color science, CDOM's absorption coefficient at 440 nm, $a_g(440)$, is often taken as the proxy of its concentration and remote sensing inversion also often returns $a_g(440)$ [*Lee*, 2006]. In our underwater continuous measurement, CDOM concentrations were measured by a fluorometer that returns voltages (V) as CDOM's proxy. In

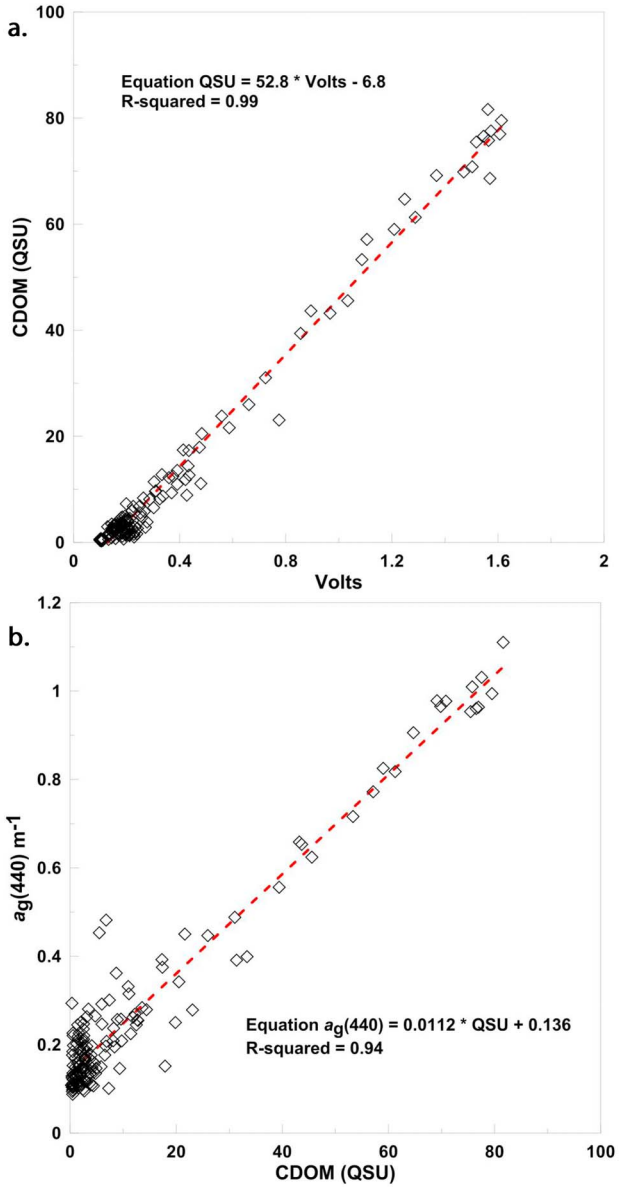

Figure 2. Correlations among CDOM's proxies, QSU, volts, and absorption coefficients $a_g(440)$. (a) Volts versus QSU. (b) QSU versus $a_g(440)$.

our discrete samples, we measured CDOM fluorescence in QSU and CDOM absorption (a_g). Those three CDOM proxies, QSU, $a_g(440)$ and instantaneous voltage, have been found strongly correlated (Figure 2). Based on these linear relationships, the voltages continuously measured can be converted to QSU or a_g.

[21] We used an empirical approach to compute in situ individual absorption properties a_g, a_d and a_{ph} from the total absorption coefficient a_t measured by AC-9, which were used to calibrate J_1 and J_2 (section 3.3) and validate inversion algorithm. Since our underwater measurement was taken at very high resolution, some water samples are high CDOM but very low chlorophyll and NAP (in chlorophyll fluorometer voltage and OBS fluorometer voltage, respectively). For these samples, the water's total absorption coefficient should be contributed almost completely by CDOM, that is, $a_t \approx a_g$, especially for short wavelength (412, 440 nm) where CDOM has relatively strong absorptions. Then for these samples, we used a_t to approximate a_g. We validated this by relating a_t to CDOM concentration in Figure 3. Figure 3a shows the samples having relatively high chlorophyll and NAP's concentrations (CHL > 1.5 mg/l, and OBS > 50 FTU) and Figure 3b shows those CDOM-dominant samples only (CHL < 0.1 mg/l, OBS < 0.1 FTU). The latter demonstrates a fairly good correlation between a_t and QSU. We then use this correlation to estimate a_g from V, as $\hat{a}_g$ derived, for all samples. After that, $\hat{a}_p$ can be obtained by $a_t - \hat{a}_g$. We further applied the similar approach to convert chlorophyll and NAP's voltages to their respective absorption coefficients (Figures 3c and 3d). For those samples with relatively high NAP but low chlorophyll, $\hat{a}_p$ should be mostly contributed by NAP. Therefore, we used $\hat{a}_p$ to approximate $\hat{a}_d$ and applied the relationship between $\hat{a}_p$ and OBS to derive $\hat{a}_d$. Finally, $\hat{a}_{ph}$ was obtained by $\hat{a}_p - \hat{a}_d$.

[22] Compared with the results of discrete sample analysis, $\hat{a}_g$ obtained by this empirical approach tends to be larger ($bias_{log}$ = 0.5) because of the minor contributions of chlorophyll, NAP and other possible in-water constituents in CDOM-dominant samples. To minimize potential uncertainties, we did not directly use these converted values $\hat{a}_g$, $\hat{a}_{ph}$ and $\hat{a}_d$, but take into account their proportions in $\hat{a}_t$, defined as the sum of $\hat{a}_g$, $\hat{a}_{ph}$, and $\hat{a}_d$. These proportions were used to partition a_t, measured by AC-9, i.e., $a_g = a_t \cdot (\hat{a}_g/\hat{a}_t)$, $a_{ph} = a_t \cdot (\hat{a}_{ph}/\hat{a}_t)$, and $a_d = a_t \cdot (\hat{a}_d/\hat{a}_t)$.

[23] In this study, the total attenuation coefficient c and the total absorption coefficient a_t were measured by AC-9. The total scattering coefficient b was calculated by subtracting absorption coefficients from attenuation coefficients, that is, $b = c - a$. Then backscattering coefficients, b_b, can be calculated by estimating the contributions of backscattering to the total scattering. Generally the proportions of b_b to b is 2% [*Kirk*, 1994], that is, $b_b = 2\% \cdot b$. Then backscattering coefficients of particles can be given by subtracting water's backscattering from the total backscattering, that is, $b_{bp} = b_b - b_{bw}$.

3.2. Quasi-Analytical Algorithm

[24] Given the water remote sensing reflectance as input, the quasi-analytical algorithm (QAA) proposed by *Lee et al.* [2002] could be used to retrieve a, b_{bp}, a_{ph}, and a_{dg} at different levels. This algorithm combines several classic empirical, semianalytical, and analytical models, which are all well known and have been fully studied and validated [*Lee et al.*, 2002]. Later, *Lee et al.* [2007] improved the empirical estimation of $a(555)$, making it more accurate and seamless. The original QAA consists of three levels with 10 steps. Starting from input of R_{rs} or r_{rs} (just below-surface remote sensing reflectance), at each level, different IOPs are estimated and applied to the next level as new inputs (Figure 4). The final output of QAA is $a_{ph}(\lambda)$ and $a_{dg}(\lambda)$, in which $a_{dg}(440)$ is often taken as CDOM's concentration. One of the merits of QAA is that it does not require the prior knowledge of aquatic constituents, since its parameters have already been synthesized for all water cases. QAA has been used in ocean color inversions with good performance [*Chang and Gould*, 2006; *Lee*, 2006; *Lee and Carder*, 2004; *Zhan et al.*, 2005]. In a recent algorithm compari-

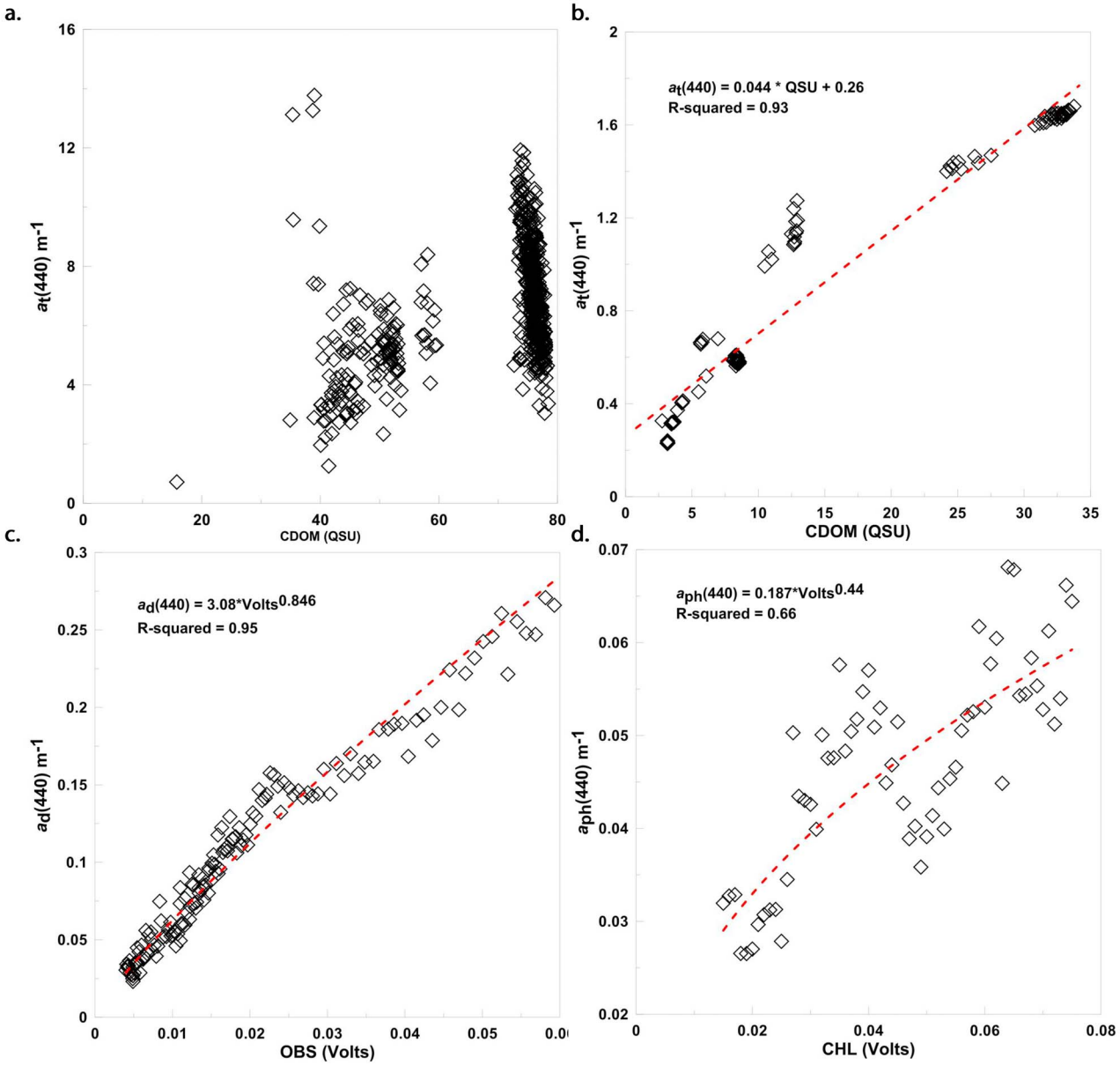

Figure 3. Separating $a_t(440)$ into three components. (a) If samples are not CDOM-dominant, there are no correlations between $a_t(440)$ and QSU. (b) For CDOM-dominant samples, the correlation between $a_t(440)$ and QSU is significant. (c) $a_d(440)$ and (d) $a_{ph}(440)$ are further separated from $a_t(440)$ using similar approaches. Note that in Figure 3b, $a_t(440)$ is approximately equal to $a_g(440)$.

son by *Qin et al.* [2007], QAA was verified to have the highest accuracy in retrieving the coefficients of total absorption and backscattering among seven other algorithms. However, they also found that when water is turbid, the accuracy of the algorithm generally degrades rapidly with increasing CDOM and NAP concentrations. Details of QAA (Version 4) are presented in Table A1 of Appendix A.

3.3. QAA-E: Separate a_g From a_{dg}

[25] At the last level, QAA separates water's total absorption coefficients into a_{ph} and a_{dg}. To retrieve CDOM concentration, a_{dg} need to be further decomposed to a_g and a_d. Due to their similar features of absorption, CDOM and nonalgal particles are difficult to distinguish from their total absorption coefficient. *Lee* [1994] has proposed an empirical separation method by making a regression fit between a_d440 and c by the formula

$$a_d(440) = 61.44\chi^{1.31}, \quad (6)$$

where χ is a parameter derived from a radiative transfer model [*Lee*, 1994]. This empirical equation (6) was only based on 39 samples collected from Mississippi River, so whether this method is appropriate for more varied water conditions and locations is not yet known.

[26] Although CDOM and nonalgal particles have the similar absorptions properties, we noticed they have completely different backscatter properties. Backscattering plays

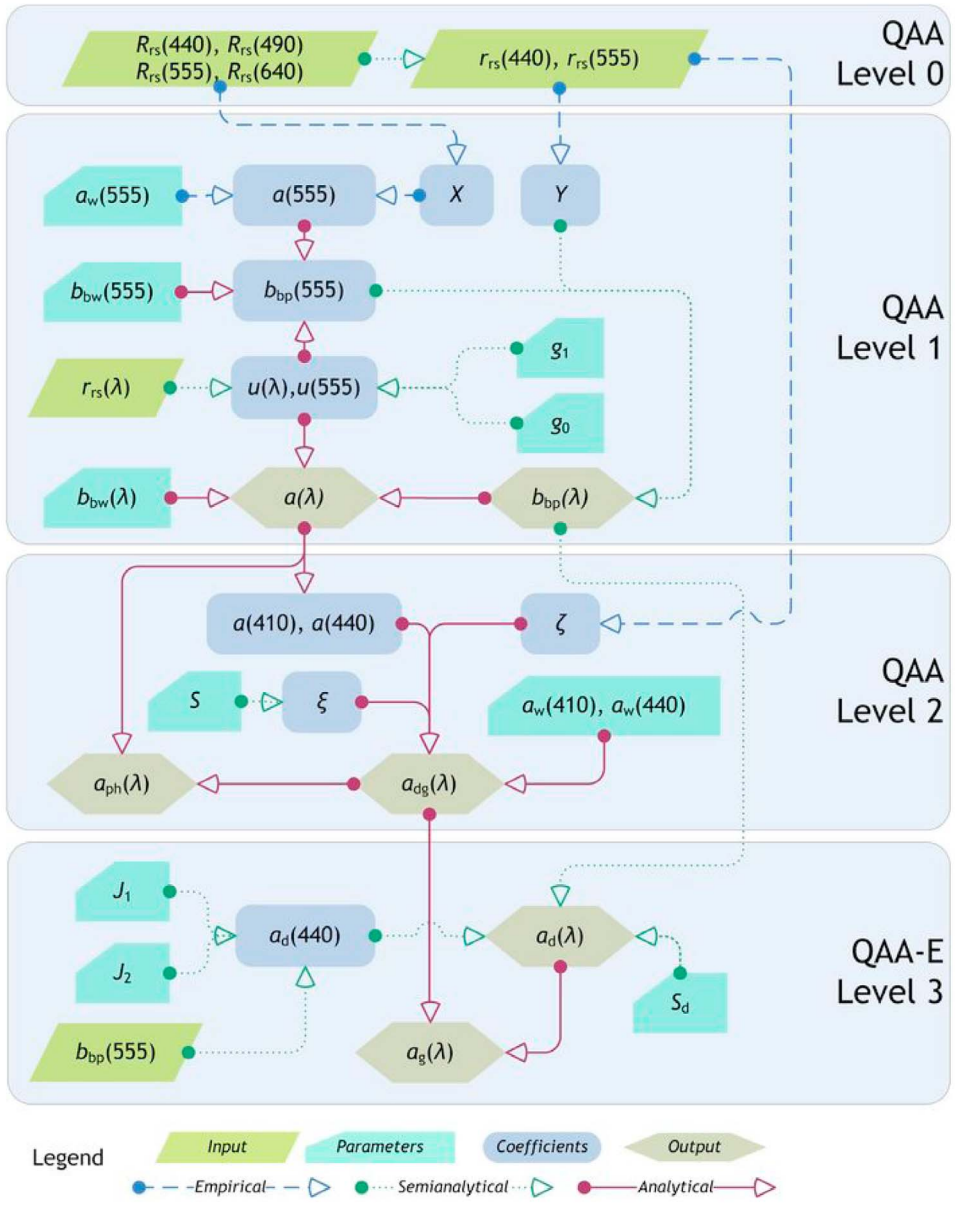

Figure 4. Concept and schematic flowchart of the level-by-level QAA and QAA-E.

the equally important role as absorption in determining remote sensing reflectance. Normally CDOM is considered to have no backscattering, whereas particles have strong backscattering, even in longer wavelength. This property inspires a semianalytical decomposition approach by estimating the nonalgal particle absorption coefficient using particulate backscattering properties.

[27] According to *Babin et al.* [2003a, 2003b], the nonalgal particulate absorption and total particulate backscattering coefficients may be represented as a function of the absorption and backscattering at a reference wavelength, respectively, that is,

$$a_d(\lambda) = a_d(\lambda_{a,ref}) \exp\left[S_d(\lambda - \lambda_{a,ref})\right] \tag{7}$$

and

$$b_{bp}(\lambda) = b_{bp}(\lambda_{b,ref}) \left(\frac{\lambda}{\lambda_{b,ref}}\right)^{Y}, \tag{8}$$

where $a_d(\lambda_{a,ref})$ and $b_{bp}(\lambda_{b,ref})$ are the specific absorption and backscattering coefficients at their respective reference wavelength, typically, $\lambda_{a,ref} = 443$ and $\lambda_{b,ref} = 555$. S_d and Y are the parameters determining their exponential decay slopes. *Babin et al.* [2003a] reported $S_d = 0.0123$ and $Y = -0.15$. S_d is very close to $S_{dg} = 0.015$ used in QAA. Y is a function of just below-surface remote sensing reflectance r_{rs} (see the equations of r_{rs} and Y in Table A1 of Appendix A). Then the relationship between a_d and b_{bp} is

$$\frac{a_d(\lambda)}{b_{bp}(\lambda)} = \frac{a_d(443)\exp[-0.015(\lambda - 443)]}{b_{bp}(555)(\lambda/555)^{Y}}. \tag{9}$$

$a_d(\lambda)$ could be derived through equation (9) as long as the $b_{bp}(\lambda)$ and the ratio $q = a_d443/b_{bp}555$ are known. In QAA, $b_{bp}(\lambda)$ is already retrieved, so we only need to determine q. a_d443 and $b_{bp}555$ are both connected to suspended particulate matter (SPM); their ratio could be derived from two equations suggested by *Babin et al.* [2003a, 2003b]:

$$a_d(443) : \mathrm{SPM} = 0.041$$

$$b_{bp}(555) : \mathrm{SPM} = 0.51$$

Therefore, we get $q = 0.0804$, namely, $a_d443 = 0.0804 b_{bp}555$. However, for ocean color components, the relationship between their optical properties and physical concentrations is often expressed by a power function. For instance, the specific absorption coefficients of chlorophyll $a_{ph}^*(440) = 0.06[C]^{0.65}$ [*Maritorena et al.*, 2000]. In addition, equation (6) implies a_d440 is a power function of a radiative transfer parameter. Based on the above consideration, if a_d443 and $b_{bp}555$ are both power functions of SPM, then q is also a power function of SPM. This equally means a_d443 could be expressed as a power function of $b_{bp}555$, that is,

$$a_d(440) = J_1 b_{bp}(555)^{J_2}. \quad (10)$$

Then coefficients J_1 and J_2 can be estimated from a least square fit. Once a_d443 is known (here assuming it is equal to a_d440), we then obtain a_g440 by subtracting a_d443 from the known $a_{dg}440$. The full flowchart and equations of QAA-E are also summarized in Figure 4 and Table A2 of Appendix A, respectively.

[28] However, according to *Babin et al.* [2003b], the relationship between a_d440 and SPM may not be accurate because the phytoplankton is a fraction of the SPM, which does not contribute to a_d440 but does to $a_{ph}440$. Therefore, the exact relationship should be created between the a_p440 (the sum of a_d440 and $a_{ph}440$) and SPM. In the same way, we can further obtain the following expression:

$$a_p(440) = J_1 b_{bp}(555)^{J_2}. \quad (11)$$

Then an alternative method to retrieve a_g440 is using

$$a_g(440) = a_t(440) - a_p(440), \quad (12)$$

where a_t440 is the total absorption coefficient for the three ocean color components. It is derived by QAA at the level 1.

[29] In this study, the above two schemes, called a_d-based and a_p-based, respectively, were both applied to retrieve a_g440. If a_{dg} is directly used to represent a_g440 without decomposition, we call it an a_{dg}-based scheme. The results of J_1 and J_2 and comparison of the three schemes are shown in section 3.4.

3.4. Accuracy Assessment

[30] Algorithm performance was evaluated using the following three statistics: the relative error, normalized bias, and root mean square error (RMSE). The former two assess systematic error, and the latter assesses random error:

$$Error_i = \frac{x_i^{model} - x_i^{obs}}{x_i^{obs}}$$

$$bias = \mathrm{Mean}(Error)$$

$$RMSE = \mathrm{Stdev}(Error),$$

where x^{model} is the variable of interest derived from proposed models or algorithms, x^{obs} is the same variable known as the truth, either observed from in situ measurement or the synthetic simulation, and "Mean" and "Stdev" are the mean and standard deviation of errors, respectively.

[31] The statistical distributions of ocean color components often follow lognormal distribution [*O'Reilly et al.*, 1998]. Therefore, the error, bias and RMSE can be also normalized as

$$Error_{\log i} = \log\left(x_i^{model}\right) - \log\left(x_i^{obs}\right)$$

$$bias_{\log} = \mathrm{Mean}\left(Error_{\log}\right)$$

$$RMSE_{\log} = \left(\frac{1}{n-2}\sum_{i=1}^{n}\left[\log\left(x_i^{model}\right) - \log\left(x_i^{obs}\right)\right]^2\right)^{\frac{1}{2}},$$

where n is the number of observations [*Lee*, 2006].

4. Results and Discussion

4.1. The Field-Measured CDOM and Water's IOPs and AOPs

[32] The field-measured CDOM demonstrated a wide range from 0.6 to 80 QSU (Figure 1b). The Atchafalaya River plume shows a steeper CDOM gradient than the Mississippi. Selected hyperspectral above-surface spectra of different water types are shown in Figure 5 (see also Table 1). The highest remote sensing reflectance reaches approximately 0.025 sr^{-1} for the waters at the Atchafalaya River mouth (SS# 46-678; SS# denotes the data set-spectrum number. Refer to Figure 1a for their sampling locations). The R_{rs} spectrum of the Atchafalaya end-member can be characterized by three minor peaks at 570 nm, 640 nm, and 690 nm. The inland sample, SS# 44-1218, presents the same three peaks. Another sample in the Atchafalaya River plume (SS# 51-1800) also has three peaks, but apparently the latter two peaks have lower R_{rs} than the first. Compared to the Atchafalaya, samples located in the Mississippi River plume (SS# 1-648, 10-2668, and 6-1511) show a relatively low remote sensing reflectance. The inland river channel (SS# 44-1218) also has higher reflectance than the Mississippi River mouth (SS# 1-648). Lower spectral reflectance magnitudes are seen farther from the coastline, for example, the three curves along the Mississippi plume: SS# 10-2668, 6-1511, and 26-3082. Very turbid waters have an additional peak near 800 nm which is induced by high concentration of suspended sediments.

4.2. Determination of the Absorption-Backscattering Relationship

[33] In QAA-E, the a_d440 is derived from the $b_{bp}555$ by the equation (10), in which parameters J_1 and J_2 were fitted

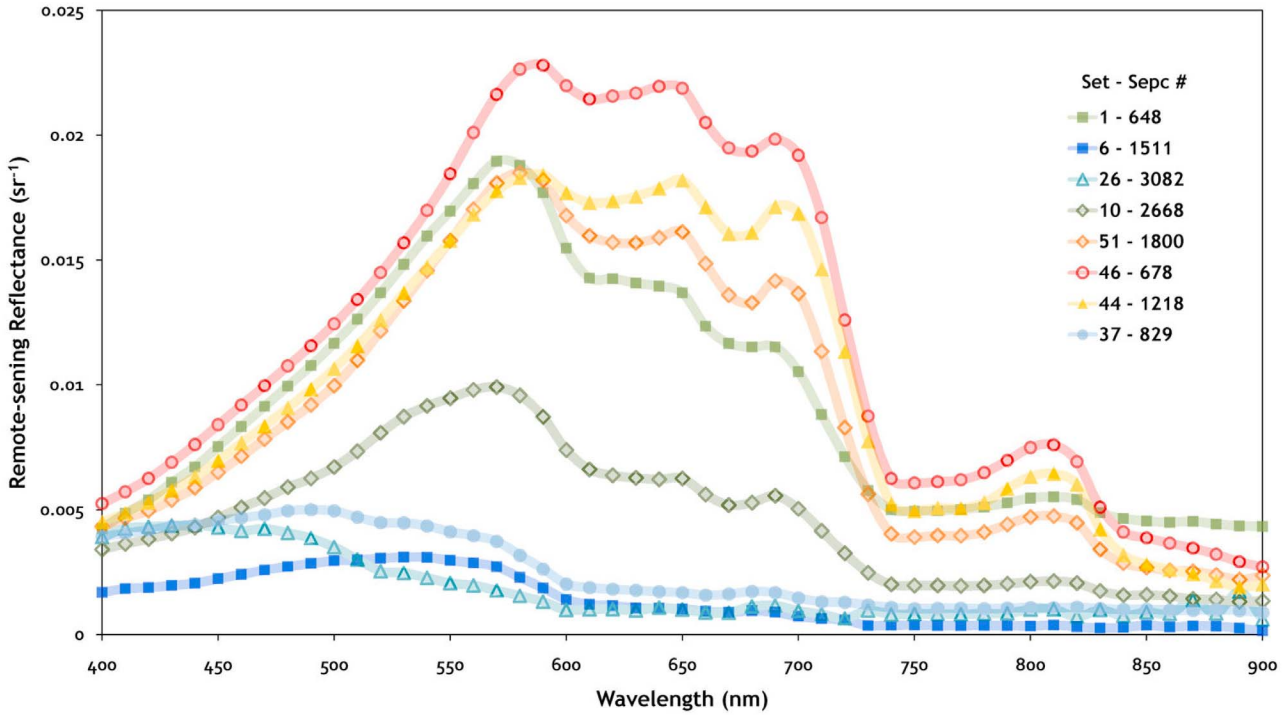

Figure 5. Selected typical hyperspectral remote sensing spectra. Each curve is labeled by set-spectrum number. Their locations are marked in Figure 1a, and water properties and IOPs are shown in Table 1.

by two data sets: the synthetic data and our field data. The synthetic data, containing 500 samples, are provided by IOCCG for ocean color algorithm testing and validation. They are simulated by Hydrolight® and cover a wide range of natural water variation.

[34] The results of least square fitting are shown in Figure 6 and Figure 7. Using IOCCG synthetic data (Figure 6), for a_d-based scheme, $J_1 = 2.355$ and $J_2 = 1.025$, with $R^2 = 0.79$; and for a_p-based scheme, $J_1 = 6.188$ and $J_2 = 0.953$, with $R^2 = 0.89$. The greater R^2 of a_p-based scheme indicates $b_{bp}555$ are better correlated to a_p440 than a_d440. Both J_2 are close to 1, implying the a_d and a_p are about linearly related to b_{bp}. The difference of J_1 from the two methods represents how much $a_{ph}440$ contributes to a_p440. Using our field data (Figure 7), for a_d-based scheme, $J_1 = 0.966$ and $J_2 = 1.038$, with $R^2 = 0.965$; and for a_p-based scheme, $J_1 = 1.026$ and $J_2 = 0.817$, with $R^2 = 0.954$. We can see that both J_1 and J_2 from two schemes are very close. This implies $a_{ph}440$ does not contribute to a_p440 significantly. J_1 and J_2 are critical parameters to derive a_d440 and a_p440, and hence a_g440. We will discuss their sensitivities regarding to the estimate accuracy of a_g440 in section 4.5.

4.3. QAA-E Test Using IOCCG Synthetic Data

[35] The results of the QAA-E test are shown in Figure 8 and Table 2. The error statistics show QAA-E performs excellently in retrieving a_g440. The a_d440's RMSE is abnormally high because a_d440s absolute values are very low and its RMSE is subjected to the effect of extreme estimates. Comparatively, the fact that the $RMSE_{log}$ is much less than the RMSE indicates in this case the $RMSE_{log}$ is much better to present random error than the RMSE.

[36] If we do not separate $a_{dg}440$, that is, use the QAA-derived $a_{dg}440$ to approximate the real a_g440, then a_g440 is apparently overestimated (Figure 8a). Figure 8c shows that a_d440 was estimated better than a_p440 (Figure 8b). After a_{dg} separation, the overestimation is well corrected, both for a_d-based and a_p-based schemes (Figures 8d–8g). The biases decreased from 0.488 to 0.174 and 0.216, (for $bias_{log}$, from 0.1488 to 0.0448 and 0.0287), respectively. By the a_d-based scheme, the RMSE also decreased from 1.116 to 0.458 (for

Table 1. The Measured Water Properties of Selected Samples[a]

Location	Set- Spectrum Number	Depth (m)	Salinity (PSU)	CDOM (QSU)	CHL (mg/l)	OBS (FTU)	a_{440} (m^{-1})	a_{555} (m^{-1})	a_{650} (m^{-1})	c_{440} (m^{-1})	c_{555} (m^{-1})	c_{650} (m^{-1})
Atchafalaya	46-678	0.83	0.29	82.21	1.40	312.91	7.068	0.263	0.080	48.98	47.18	39.66
Atchafalaya	51-1800	0.41	0.23	78.62	1.14	212.18	3.663	0.991	0.282	49.10	36.68	32.28
Mississippi	1-648	0.19	6.47	31.96	0.01	0.06	1.644	0.360	0.106	10.27	7.634	6.462
Mississippi	10-2668	3.29	30.41	6.30	0.73	8.78	0.634	0.166	0.049	4.32	3.500	3.113
Mississippi	6-1511	24.80	36.20	2.91	0.18	0.01	0.351	0.113	0.032	3.23	2.810	2.582
Gulf	37-829	6.93	34.15	1.99	0.37	1.23	0.327	0.088	0.023	3.08	2.792	2.659
Gulf	26-3082	16.95	36.25	0.77	0.07	0.07	0.192	0.060	0.015	2.17	2.044	1.979

[a]No ECOShuttle data for the inland water sample 44-1218.

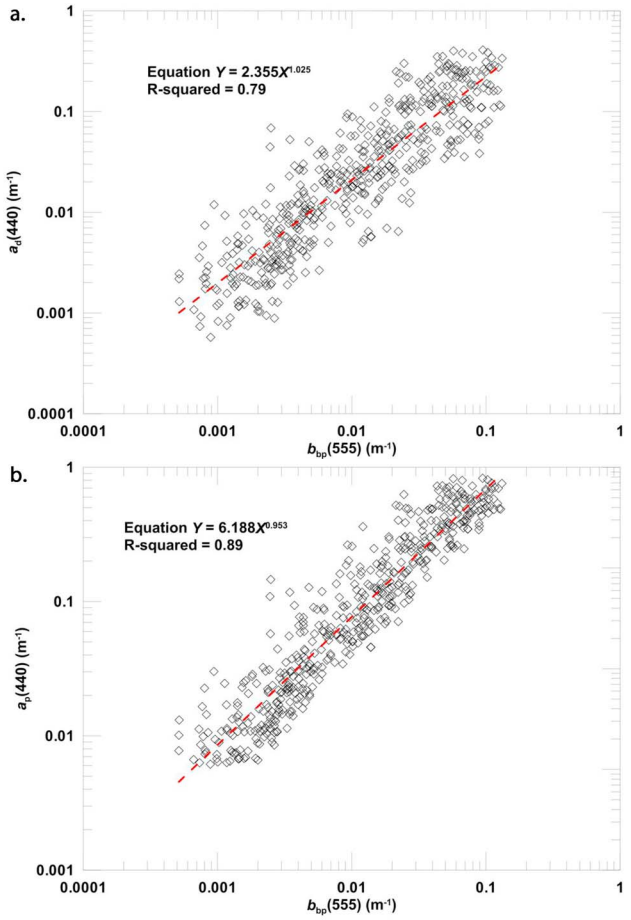

Figure 6. Relationships between $b_{bp}555$ and (a) a_d440 and (b) a_p440, using synthetic data. Their equations are fitted as $a_d440 = 2.355b_{bp}^{1.025}$ ($R^2 = 0.79$) and $a_p440 = 6.188b_{bp}^{0.953}$ ($R^2 = 0.89$), respectively.

the $RMSE_{log}$, from 0.206 to 0.155), but by the a_p-based scheme, the RMSE is slightly worse than that without separation. The a_d-based scheme returns 498 valid outcomes (positive values) whereas the a_p-based only returns 485. As to R^2, the a_d-based scheme keeps the same R^2 and R^2 II (R-squared determination for regression type II) as the a_{dg}-based scheme, while the a_p-based scheme has a higher R^2 but lower R^2 II. We plot their results in Figure 8d and Figure 8f in log scale and Figure 8e and Figure 8g in linear scale, respectively. By comparisons, the a_d-based scheme performs better than the a_p-based scheme for low a_g440 (around 0.01 m^{-1}) but worse for high a_g440 (around 2 m^{-1}). Although theoretically the a_p-based scheme is more ideal than the a_d-based, actually the a_d-based scheme performs a little better than the a_p-based overall, except the $bias_{log}$ and R^2 II. We think this may be caused by the phytoplankton which introduces more uncertainty into the a_p440.

[37] Beside the above accuracy statistics, the a_d-a_{dg} ratio was also used to assess the performance of QAA-E. An assumption for a_{dg} separation is that a_d takes significant proportion in a_{dg}. In this study, we set the ratio = 0.1 as the condition that the a_{dg} should be separated. The ratio of the synthetic data ranges from 0.019 to 0.74 with the average 0.21 and follows a lognormal distribution (Figure 9a). As the inversion results, the derived a_d-a_{dg} ratio has very similar range (from 0.015 to 0.84 with average 0.19) and distribution (Figure 9b). The detailed comparison (from 0.1 to 0.7 with interval 0.02) between the measured and derived a_d-a_{dg} ratios also shows they match very well (Figure 9c).

[38] We also analyzed the relationship between prediction error and a_d-a_{dg} ratio. The results show that when the ratio is low (0.1–0.4), the error (bias) is also low (Figure 10a); but as the ratio is high, most errors tend to be positive and hence make a large bias. This phenomenon implies that the QAA-E works well for moderate a_d-a_{dg} ratios, but for very large a_d-a_{dg} ratios further refinement is required. The very large a_d-a_{dg} ratio means the sediment concentration is extremely high and in this case the water optical properties are very complicated. The remote sensing inversion of a_g for such water remains challenging.

4.4. QAA-E Test Using IOCCG in Situ Data

[39] The synthetic data test shows QAA-E is able to separate $a_{dg}440$ effectively and hence improve the accuracy of CDOM's inversion. We also applied QAA-E to the IOCCG in situ data set which was collected by 11 experiments, 656 stations, throughout the global oceans, mostly sampled in coastal areas. This in situ data set only provides $a_{dg}440$ and $a_{ph}440$, so we were unable to validate the accuracy of the inverted a_g440. Nevertheless, we can still evaluate a_d-a_{dg} ratio using QAA-E-derived a_d440 and in situ $a_{dg}440$. In the test, J_1 and J_2 were set by the values

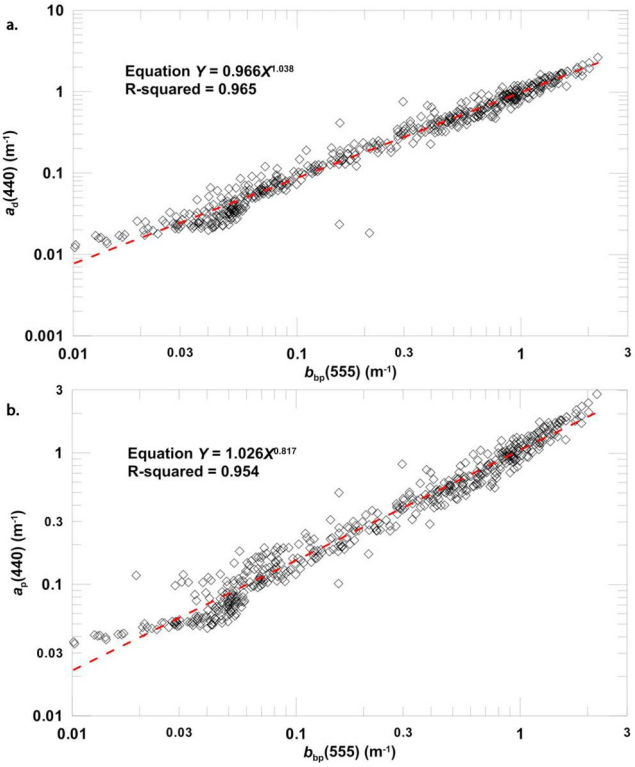

Figure 7. Relationships between $b_{bp}555$ and (a) a_d440 and (b) a_p440, using the measured in situ data. Their equations are fitted as $a_d440 = 0.966b_{bp}^{1.038}$ ($R^2 = 0.965$) and $a_p440 = 1.026b_{bp}^{0.817}$ ($R^2 = 0.954$), respectively.

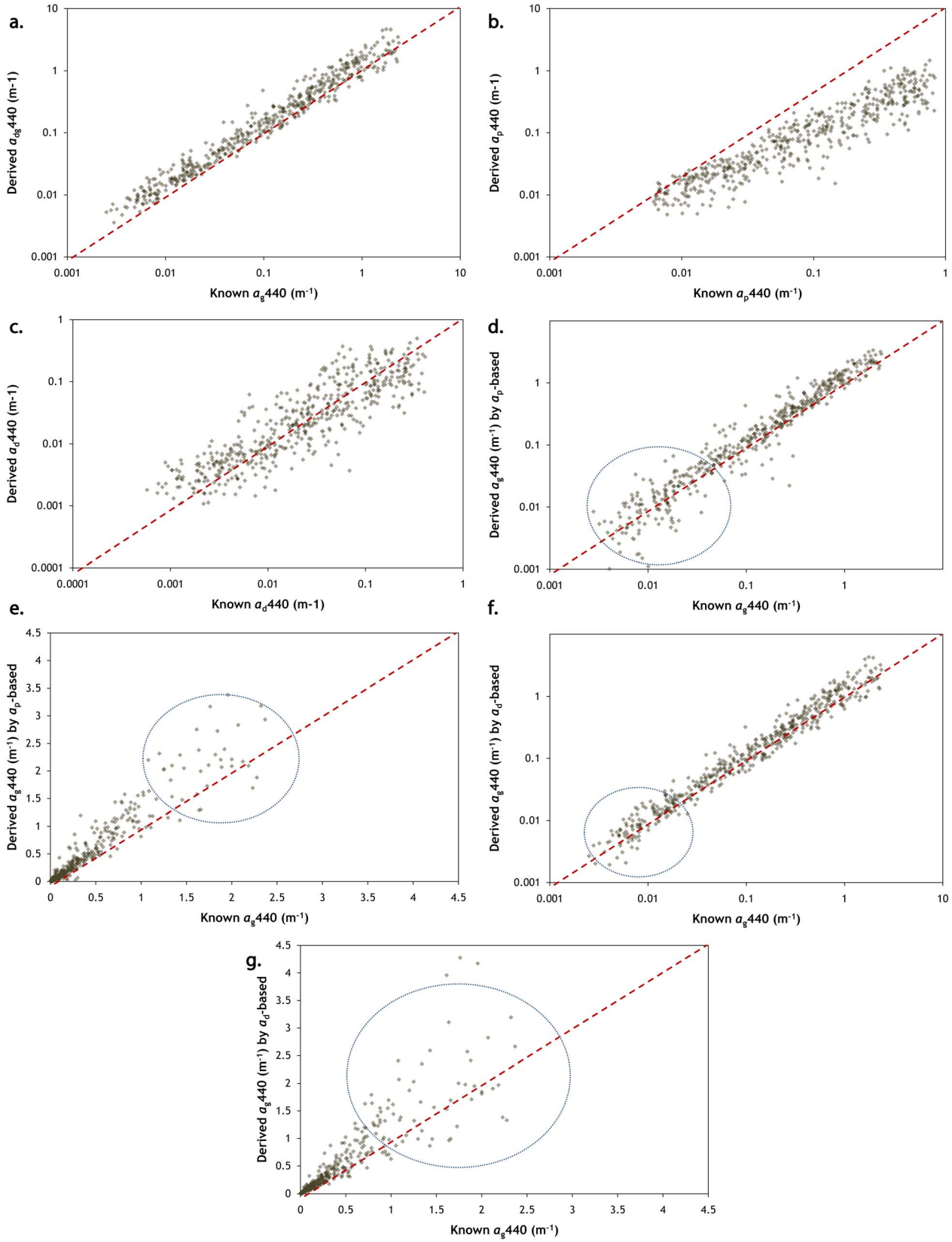

Figure 8. QAA-E test using IOCCG synthetic data. (a) The a_{dg}-based scheme, namely, without a_{dg}440 separation, (b) a_p440, (c) a_d440, and (d-g) all resultant a_g440, where Figures 8d and 8e are a_p-based and Figures 8f and 8g are a_d-based. Note that Figures 8d and 8f are plotted in log scale and Figures 8e and 8g are in linear scale.

Table 2. Summary of Error Analysis for QAA and QAA-E, Using Synthetic and in Situ Data[a]

	N	n	R^2	R^2 II	bias	RMSE	$\text{bias}_{\log}$	$\text{RMSE}_{\log}$
IOCCG Synthetic Data								
a_t	500	500	0.92	0.99	0.140	0.107	0.0522	0.082
b_{bp}	500	500	0.92	0.99	0.026	0.081	0.0045	0.074
a_p	500	500	0.67	0.87	0.136	0.437	0.0042	0.225
a_d	500	500	0.45	0.76	0.359	4.737	0.0047	0.341
a_{dg}	500	500	0.81	0.98	0.131	0.248	0.0389	0.118
a_{g1}	500	498	0.81	0.97	0.174	0.458	0.0448	0.155
a_{g2}	500	485	0.91	0.92	0.216	1.201	0.0287	0.256
a_{g3}	500	500	0.80	0.97	0.488	1.116	0.1488	0.206
In Situ Data of Atchafalaya and Mississippi River Plumes								
a_t	3010	3010	0.71	0.69	−0.418	0.103	−0.252	0.278
b_{bp}	3010	2996	0.88	0.55	−0.913	0.095	−1.142	1.177
a_p	3010	2996	0.23	0.36	−0.524	8.064	−0.419	0.473
a_d	3010	2996	0.29	0.48	−0.495	2.264	−0.407	0.495
a_{dg}	3010	3010	0.70	0.59	−0.484	0.117	−0.306	0.330
a_{g1}	3010	2996	0.65	0.53	−0.473	0.120	−0.299	0.327
a_{g2}	3010	2996	0.64	0.63	−0.323	0.138	−0.188	0.222
a_{g3}	3010	3010	0.71	0.58	−0.443	0.112	−0.273	0.299

[a]The absorption coefficients and backscattering coefficients are at 440 and 555 nm, respectively. a_{g1}, a_{g2}, and a_{g3} refer to a_g derived by a_d-based, a_p-based (QAA-E), and a_{dg}-based algorithms (QAA), respectively. N is the number of input samples, and n is the number of samples with valid output.

derived from the synthetic data. Among the 656 samples, only one sample returns an invalid a_d440 that is slightly higher than the corresponding $a_{dg}440$. For the remaining 655 samples in Figure 11a, QAA-E is well able to capture the characteristic of a_d-a_{dg} ratio observed from the synthetic data—not only the range (0.013–0.95) and average (0.15), but also a perfect lognormal distribution (Figure 11b). The derived a_d-a_{dg} ratios were also mapped, presenting a reasonable distribution (Figure 11c). Most of the samples with the ratio greater than 0.1 are found in the regions close to estuaries and coasts, where the concentrations of nonalgal sediments are assumed relatively higher than in the open oceans. We noticed the a_d-a_{dg} ratio is relatively low for the experiment LMER-TIES (Figure 11a), located at the Chesapeake Bay. Here the measured a_{dg} and derived a_d are both relatively higher than other experiments but the a_d-a_{dg} ratio is lower, indicating a_g440 dominates the $a_{dg}440$ in spite of a large a_d440. In all, the high a_d-a_{dg} ratios most likely occur in coastal and estuarine regions, but waters in those regions are not always with high a_d-a_{dg} ratios.

4.5. Sensitivity Analysis of J_1 and J_2

[40] Two new parameters, J_1 and J_2, were introduced into QAA-E, and their values were obtained by fitting known data. They play an important role in determining a_d440 or a_p440, and hence have an effect on the prediction accuracy of a_g440. A sensitivity analysis was conducted in order to test how they influence the final results. Four statistical variables, valid number n, R^2, bias, and RMSE, were used in the analysis. Fitting IOCCG synthetic data, in a_d-based scheme, resulted in $J_1 = 2.355$ and $J_2 = 1.025$; while by fitting in situ data, we got $J_1 = 0.966$ and $J_2 = 1.038$. These results imply that the a_d440 and $b_{bp}555$ are approximately linearly related but the slope may vary. Based on the above values, in this sensitivity analysis, the range of J_1 was set from 0.5 to 4.5 with interval 0.02, and that of J_2 was from 0.5 to 1.5 with interval 0.01, so for each statistic variable, in total we tested 20,000 combinations of J_1 and J_2.

[41] The results of sensitivity analysis on the synthetic data are shown in Figure 12. The valid number n is the number of samples with derived $a_{dg}440$ greater than a_d440 (i.e., positive $\hat{a}_g440$). Figure 12a shows J_2 is critical to the valid number n. When $1 < J_2 < 1.5$, n almost keeps a constant 500 within the J_1's full range 0.5–4.5, that means in their ranges, all 500 samples were derived validly. Note that n indicates how robust the inverse algorithm is to a wide range of environments. R^2, bias, and RMSE were all calculated based on the valid results. If n is much less than the amount of input data, the algorithm does not perform well even if the other three variables look good. The ranges of J_1 and J_2 for R^2 (Figure 12b) is similar to the case of n. In J_2's range 1–1.5, RMSE ranges from 0.35 to 0.5, and small J_2 and large J_1 make a relatively low RMSE (Figure 12c). Similarly, the best J_2 which leads to bias = 0 is around 0.8–0.9. Given J_2 is set, the bias is not sensitive to J_1 (Figure 12d).

[42] The same analysis was also applied to our in situ data as well as the a_p-based scheme, and we obtained similar results. We therefore can conclude that for a_d-based scheme, the derived results (a_g440) are not sensitive to valid ranges of J_1 and J_2: $0.5 < J_1 < 4.5$ and $1.0 < J_2 < 1.5$. Within the two ranges, J_1 is less sensitive than J_2. Moreover, a large J_1 and a small J_2 tend to make QAA-E return relatively better results. For the a_p-based scheme, the ranges are $0.5 < J_1 < 8.5$ and $0.8 < J_2 < 2.0$.

4.6. Inversion of a_g440 Using Field Spectral Data

[43] The QAA-E was finally applied to estimate CDOM concentrations in the Mississippi and Atchafalaya river plume regions. The results are shown in Figure 13 and Table 2. The a_t440 and $a_{dg}440$ were derived by the original QAA (Figures 13a and 13b), and the others were derived by QAA-E (Figures 13c–13g). There are 3,010 above-surface spectra used in the inversion and most of them, 2996 samples, returns valid results.

[44] In general, the accuracy of CDOM estimation is good. Using the a_d-based scheme, the a_g440's RMSE is about 0.12 ($\text{RMSE}_{\log} = 0.32$). The a_p-based scheme also performs well with RMSE = 0.138 and $\text{RMSE}_{\log} = 0.222$. However, their biases are a little larger than our expectation. We noticed that a_t440, $a_{dg}440$ and $b_{bp}555$ also have large biases, a type of systematic error. That these biases are all negative indicates they are all underestimated. Therefore, the same underestimation for the derived a_g440 may not be caused by QAA-E algorithm but likely by a_t440, $a_{dg}440$, or $b_{bp}555$ derived by QAA. The possible source of systematic errors and uncertainties are discussed in the section 4.7. Similar to the synthetic data, a_g440 are predicted more accurate than a_p440 and a_d440 (Figures 13c and 13d) but the difference is that the a_p-based scheme performs a little better than the a_d-based. Note that the result that the a_{dg}-based scheme also well estimates the a_g440 does not mean the a_{dg} separation is unnecessary. Since the a_{dg}-based scheme is assumed to overestimate the a_g440, if the systematic bias underestimates a_g440, then the final results appear better, because coincidentally the overestimation and underestimation are counteracted.

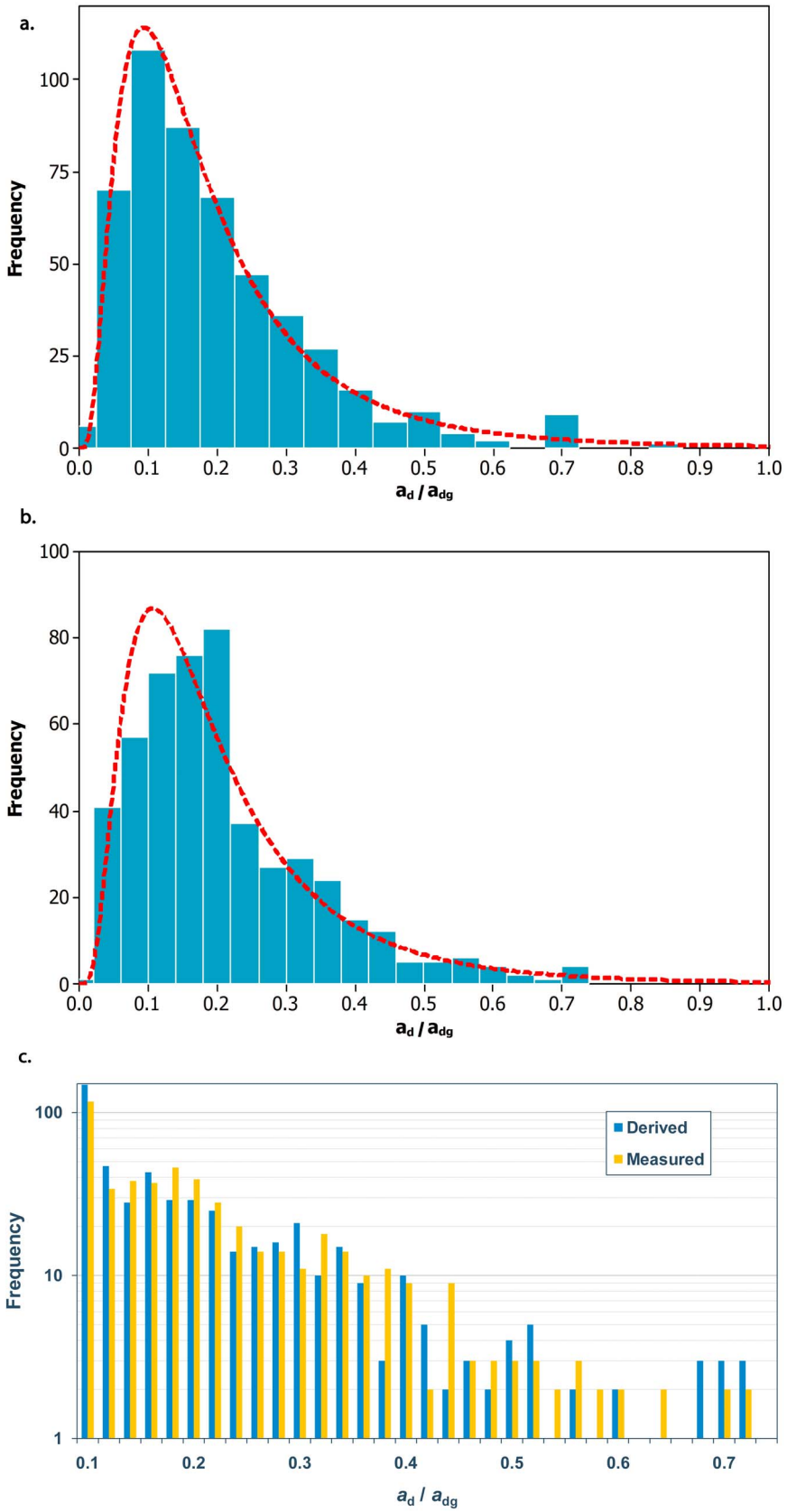

Figure 9. Compositions of $a_{dg}(440)$ (a_d-a_{dg} ratio) for (a) measured ratios of IOCCG synthetic data and (b) derived ratios using QAA-E. (c) The detailed comparison (from 0.1 to 0.7 with interval 0.02) between them.

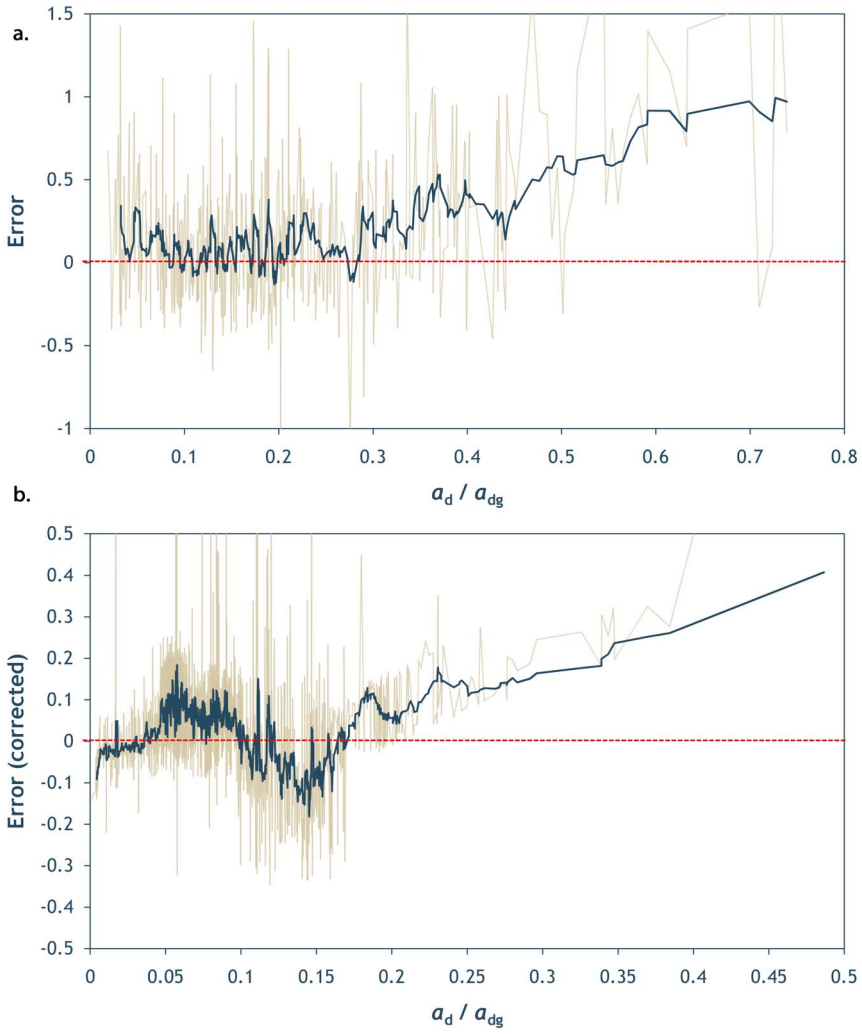

Figure 10. Inverse errors versus a_d-a_{dg} ratios. (a) IOCCG synthetic data. (b) Our in situ data. Note that errors were corrected by removing inherent errors introduced by QAA-derived $a_{dg}(440)$.

[45] The distribution of derived a_d-a_{dg} ratios also implies the good performance of QAA-E, because the ratio is less subjected to systematic error. For this study, a_d440 and a_g440 are both underestimated due to the systematic error of a_t440. When a_d-a_{dg} ratio is calculated, the systematic error is able to be canceled. Figure 14 shows for about 1,700 samples, the derived ratio, from 0.1 to 0.4 with a 0.01 interval, matches the measured ratio very well, except only a few samples with large ratios. The error versus a_d-a_{dg} ratio is plotted in Figure 10b. Due to the systematic error we mentioned above, we can see that most errors are negative. There is still a potential trend that errors become larger as the ratio increases.

4.7. Model Uncertainty and Future Work

[46] First, the uncertainty may come from the data measurement and preprocessing. At high CDOM concentrations above about 70 QSU, an "inner filter" effect is seen in the in situ fluorescence measurement. Dilution of discrete samples confirms this [*Green and Blough*, 1994]. With underway fluorescence sensor, correction through dilution is not viable. However, if the geometry of the in situ fluorometer, the excitation and emission wavelengths of sensor, and the absorption spectrum of the water are known, a correction to the in situ data can be made. *Gardner et al.* [2005] examined this issue in the Neponset Estuary. Using the same equation for inner filter effect, there would be a about a 10% effect on the most highly concentrated CDOM samples in the Atchafalaya. In this study, 1.6% of measures have CDOM concentration higher than 70 QSU, so the error should not be significant for our conclusion. Another possible factor is the depth effect. In the entire cruise, the high resolution underwater sampling of water's IOPs was carried out at inconsistent depth varying at a wide range from 0.2 to 30 m. From the surface to deep water, in situ CDOM concentration and water's IOP might show a strong variation. However, water radiance received by above surface sensor is a cumulative effect of the entire water optical column. Therefore the depth of field IOP measurement might contribute to uncertainty of IOP prediction. Since the depth profiles of water's IOPs are complex and vary with water cases and even locations, it is challenging to convert a CDOM measure at one depth to another comparable standard depth across all samples. In addition, the computation

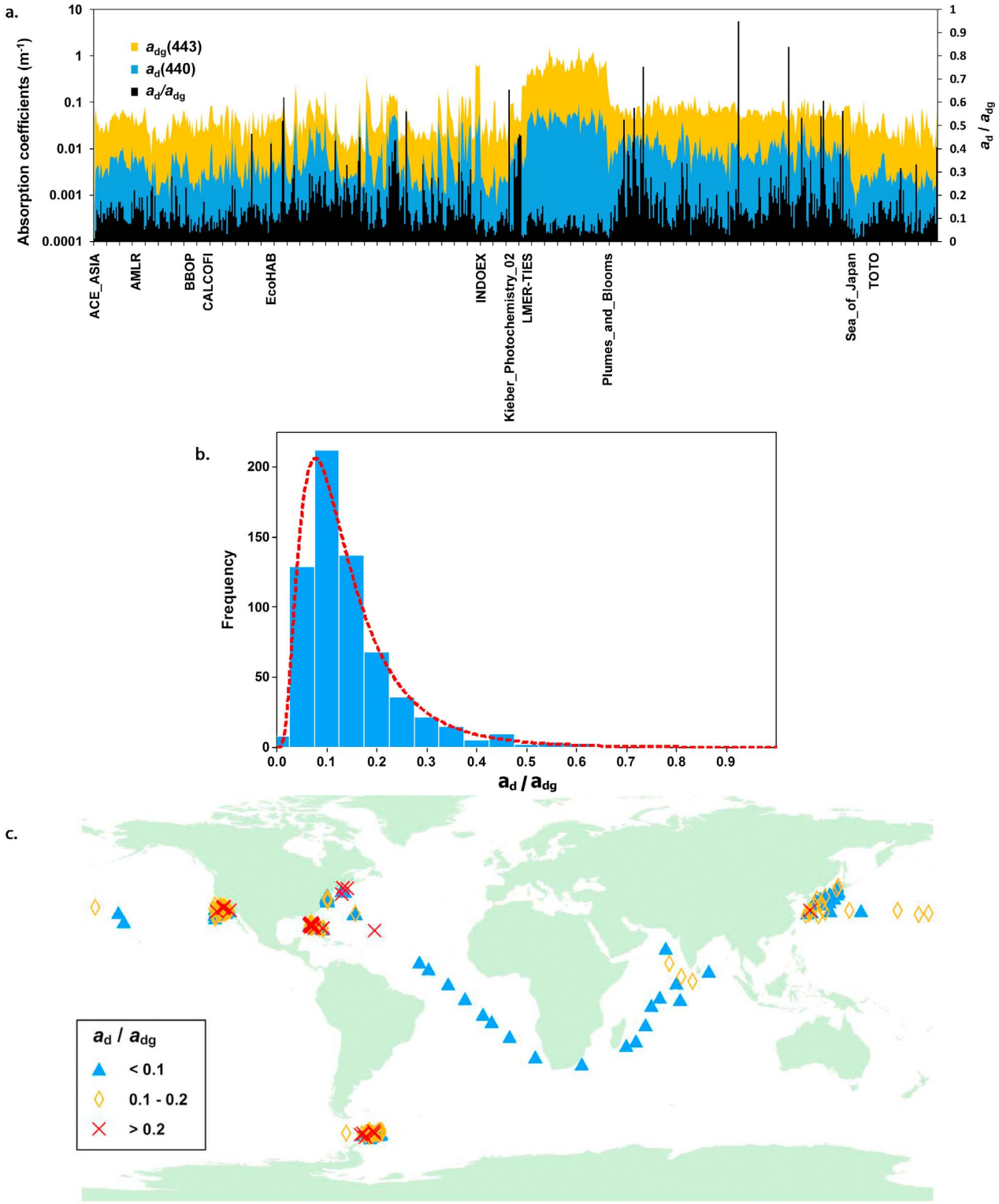

Figure 11. The ratio of $\hat{a}_d440/a_{dg}440$ and their worldwide locations. (a) The $a_{dg}440$ are in situ data provided by IOCCG and measured by 11 experiments, and $\hat{a}_d440$ are derived from a_d-based QAA-E algorithm, which returns 655 valid $\hat{a}_d440$ for the total 656 samples input. (b) Statistical distribution of $\hat{a}_d440/a_{dg}440$ follows a perfect lognormal distribution with an average of 0.15. (c) Sample geographical locations: most samples with the ratio > 0.2 locate in or near estuarine or coastal regions, where non-algal particles are often richer than open oceans.

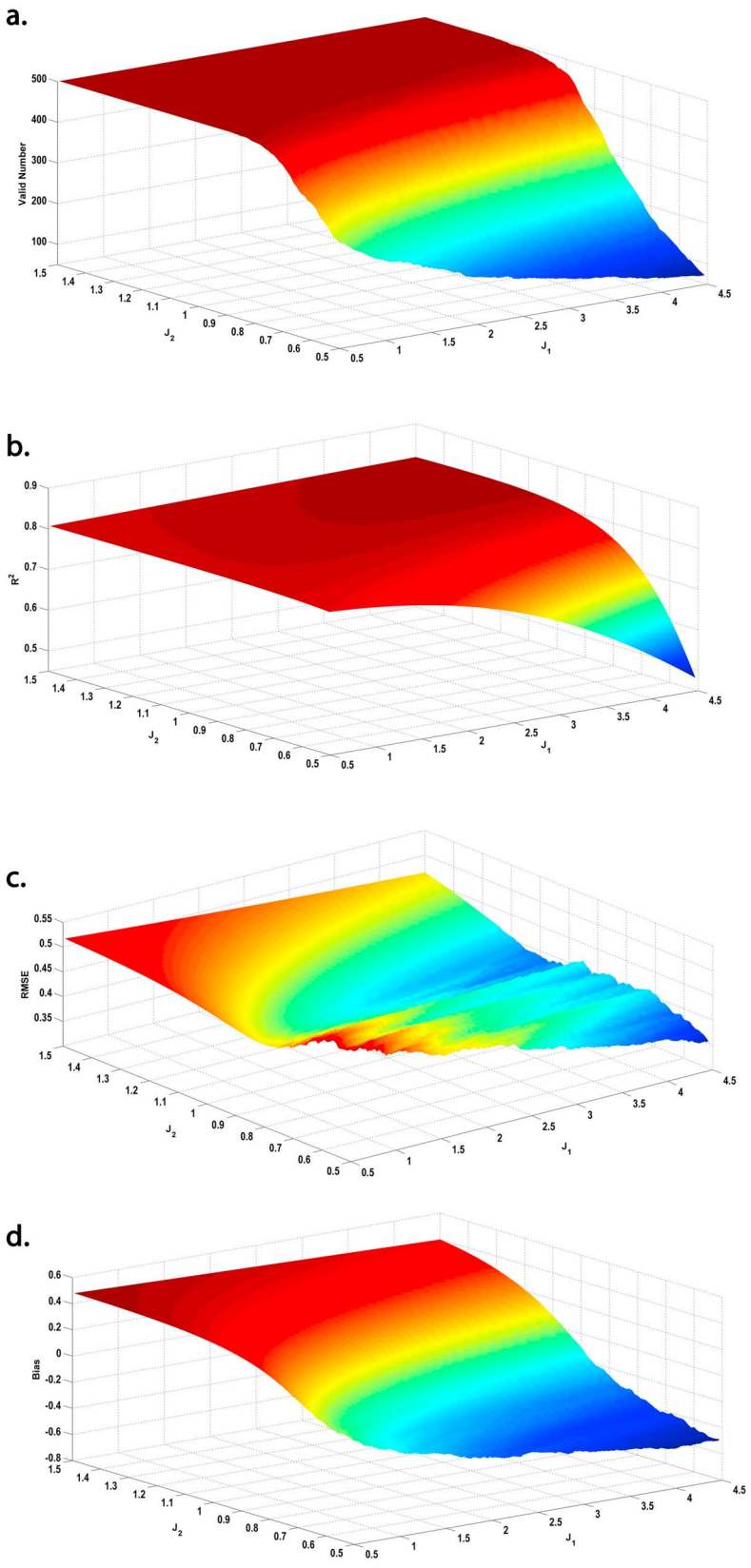

Figure 12. Sensitivity analysis for parameters J_1 and J_2, using IOCCG synthetic data and a_d-based QAA-E. Four statistic variables are evaluated: (a) valid number n, (b) R^2, (c) RMSE, and (d) bias. The results indicate the robust ranges of the two parameters are $0.5 < J_1 < 4.5$ and $1 < J_2 < 1.5$, respectively.

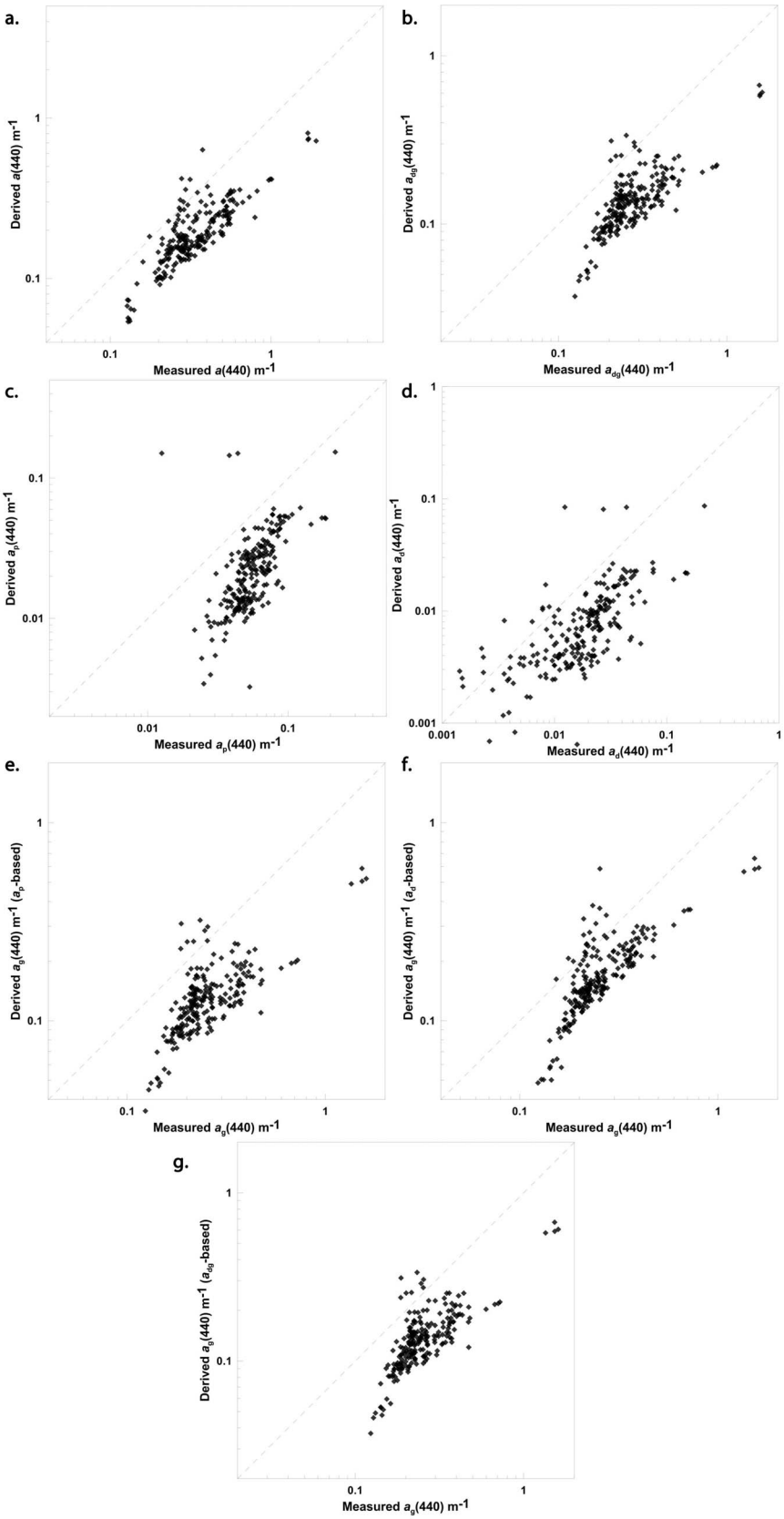

Figure 13. Comparison between QAA-derived (a) a_t440 and (b) $a_{dg}440$, and QAA-E-derived (c) a_p440, (d) a_d440, (e) a_p-based a_g440, (f) a_d-based a_g440, and (g) a_{dg}-based a_g440, using in situ data.

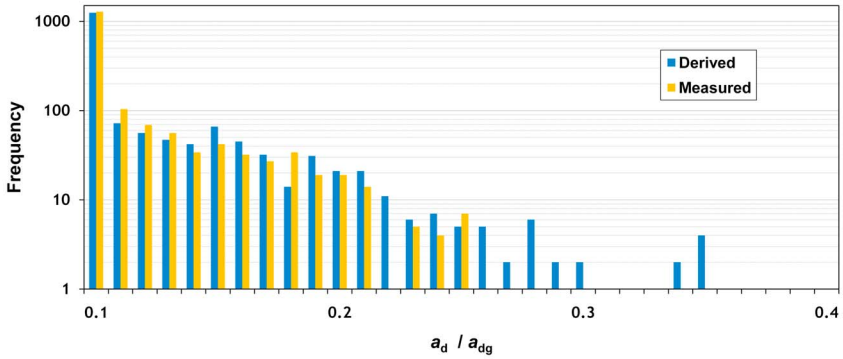

Figure 14. The measured and derived a_d-a_{dg} ratios, using our in situ data.

of individual absorption coefficients from ocean color fluorescence voltages and the total absorption coefficient measured by AC-9 may lead to uncertainty. Those individual absorption coefficients have been used to estimate J_1 and J_2 and to validate the inversion algorithm. In general, this uncertainty is expected to be small given J_1 and J_2 are not sensitive parameters.

[47] Second the uncertainty may come from the inverse algorithms. The QAA is not specially designed for Case 2 water, and some parameters used in QAA compromise for Case 1 and Case 2. Therefore, for the Mississippi and Atchafalaya Case 2 waters, it may lead to large errors. Moreover, the Case 2 water itself is more complicated than Case 1 and is not well simulated by current ocean color remote sensing models. Some uncertainty is probably induced by QAA-E because the relationship between a_d440 or a_p440 and $b_{bp}555$ may be more complex than an exponential function we have used in this study. Particularly the a_p-based method uses one function to summarize two relationships, a_d440 versus b_{bp} and $a_{ph}440$ versus b_{bp}. The latter has not been well understood. Although theoretically b_{bp} is more closely connected to a_p, it does not necessarily mean a_p is more accurately estimated than a_d based on simple functions like equation (10) and equation (11). The optical properties of phytoplankton are more complicated due to the diversity of phytoplankton and the relationship between a_{ph} and therefore b_{bp} may not be well represented by a simple exponential function as equation (11). On the other hand, the contribution of phytoplankton to b_{bp} is much smaller than that of inorganic particles. Under certain circumstance, it is possible that using one function to capture the relationship between the combined absorption coefficient a_p and b_{bp} (a_p) would lead to more error than simply ignoring a_{ph}. Additionally, although the two parameters J_1 and J_2, given in their preset ranges, are not very sensitive to the data set, the worst J_1 and J_2 may still bring a relatively large error. Therefore in future work, it would be ideal to calibrate coefficients J_1 and J_2 by local data.

[48] The third uncertain factor is remote sensing reflectance R_{rs}, which cannot be directly measured but derived by removing the simulated water surface reflectance. The surface reflectance simulation by Hydrolight® might bring some errors due to its inherent model uncertainty and approximation of input parameters, such as using average

Table A1. Steps of the QAA (Version 4) to Drive Absorption Coefficients a, a_{ph}, a_{dg}, and Backscattering Coefficient b_{bp}[a]

Step	Property	Math Formula	Approach
0	r_{rs}	$r_{rs} = R_{rs}/(0.52 + 1.7R_{rs})$	semianalytical
1	$u(\lambda)$	$u(\lambda) = \frac{-g_0+\left[g_0^2+4g_1 r_{rs}(\lambda)\right]^{\frac{1}{2}}}{2g_1}$	semianalytical
2	$a(555)$	$a(555) = a_w(555) + 10^{-1.226-1.214\chi-0.35\chi^2}$, $\chi = \log\left(\frac{R_{rs}(440)+R_{rs}(490)}{R_{rs}(555)+2\frac{R_{rs}(640)}{R_{rs}(490)}R_{rs}(640)}\right)$	empirical
3	$b_{bp}(555)$	$b_{bp}(555) = \frac{u(555)a(555)}{1-u(555)} - b_{bw}(555)$	analytical
4	Y	$Y = 2.2\{1 - 1.2\exp[-0.9\frac{r_{rs}(440)}{r_{rs}(555)}]\}$	empirical
5	$b_{bp}(\lambda)$	$b_{bp}(\lambda) = b_{bp}(555)(\frac{555}{\lambda})^Y$	semianalytical
6	a(λ)	$a(\lambda) = \frac{[1-u(\lambda)]\left[b_{bw}(\lambda)+b_{bp}(\lambda)\right]}{u(\lambda)}$	analytical
7	$\zeta = a_{CHL}(410)/a_{CHL}(440)$	$\zeta = 0.71 + \frac{0.06}{0.8+r_{rs}(440)/r_{rs}(555)}$	empirical
8	$\xi = a_{dg}(410)/a_{dg}(440)$	$\xi = \exp[S(440 - 410)]$	semianalytical
9	$a_{dg}(440)$	$a_{dg}(440) = \frac{[a(410)-\zeta a(440)]}{\xi-\zeta} - \frac{[a_w(410)-\zeta a_w(440)]}{\xi-\zeta}$	analytical
10	$a_{CHL}(440)$	$a_{CHL}(440) = a(440) - a_{dg}(440) - a_w(440)$	analytical

[a]Parameters are suggested as $g_0 = 0.0895$, $g_1 = 0.1247$, and $S = 0.015$. $a_w(\lambda)$ and $b_{bw}(\lambda)$ are absorption coefficient and backscattering coefficient of pure water at wavelength λ, respectively.

Table A2. Extended Steps of QAA (a_d-Based) to Separate a_{dg} Into a_d and a_g[a]

Step	Property	Math Formula	Approach
11	$a_d(440)$	$a_d(440) = J_1 b_{bp}(555)^{J_2}$	semianalytical
12	$a_d(\lambda)$	$a_d(\lambda) = a_d(440)\exp[S_d(\lambda - 440)]$	semianalytical
13	$a_g(\lambda)$	$a_g(\lambda) = a_{dg}(\lambda) - a_d(\lambda)$	analytical

[a]Parameters are suggested as $J_1 = 10.51$, $J_2 = 1.56$, and $S_d = -0.0123$.

wind speed over half hour as instantaneous value. How to measure and obtain R_{rs} as accurate as possible remains an important topic for future research.

5. Conclusion

[49] Very high resolution data of inherent and apparent optical properties of seawater were collected in the Mississippi and Atchafalaya river plumes. These data reveal considerable variability in these regions. Above-surface hyperspectral remote sensing data were used to observe ocean color characteristics of seawater, and CDOM concentrations were estimated using the remote sensing data. The different combinations of three ocean color components lead to the different shapes of the remote sensing reflectance observations. For turbid waters containing very high CDOM, chlorophyll and detrital particles, three peaks at 570 nm, 640 nm, and 690 nm were observed in addition to a relatively low peak at 800 nm.

[50] Based on known semianalytical models and our in situ data, the relationship between a_d440 (or a_p440) and $b_{bp}555$ was determined with an exponential function a_d440 (or a_p440) = $J_1 b_{bp}(555)^{J_2}$. Consequently, based on QAA, QAA-E was developed with three extended steps to decompose a_{dg} to a_d and a_g, either using a_d-based or a_p-based methods. Our results show that (1) QAA-E performs well in separating a_g from a_{dg}, and the a_d-based method performs a little better than the a_p-based method, and (2) the retrieved a_g estimates show excellent correspondence to in situ measurement ($R^2 = 0.65$) while providing the additional retrieval of a_d simultaneously. More insightful understanding on CDOM and particulate optical properties is required to further improve the algorithm, particularly for retrieving a_d.

[51] This study provides a successful approach for using above-surface remote sensing to accurately estimate CDOM concentrations. Our future work will focus on evaluating QAA-E's capability of estimating CDOM from satellite imagery. QAA-E uses R_{rs} or r_{rs} at the same wavelength as QAA does. Therefore, the QAA-E is applicable to all satellite images that QAA could handle.

Appendix A

[52] Based on the work of *Lee et al.* [2002, 2007], the latest QAA (version 4) and QAA-E algorithms are organized into the steps shown in Tables A1 and A2, given input data with the remote sensing reflectance measured either above surface, R_{rs}, or below surface, r_{rs} (values at or around 440 nm, 490 nm, 555 nm, and 640 nm are required).

[53] **Acknowledgments.** This research is supported by a University of Massachusetts Amherst FRG grant (21644, PI: Q. Yu), an Office of Naval Research grant (N000140910346, PI: R. F. Chen), and a collaborative NSF grant (1025547, PI: Q. Yu; 1025546, PI: Y. Q. Tian). We thank Wei Huang and Keith Ciliano at the University of Massachusetts Boston for sampling and analyzing discrete samples.

References

Amon, R. M. W., and R. Benner (1994), Rapid cycling of high-molecular-weight dissolved organic matter in the ocean, *Nature*, *369*, 549–552, doi:10.1038/369549a0.

Arrigo, K. R., C. R. McClain, J. K. Firestone, C. W. Sullivan, and J. C. Comiso (1994), A comparison of CZCS and in situ pigment concentrations in the Southern Ocean, *NASA Tech. Memo., NASA TM-104566*, vol. 13, 30–34.

Analytical Spectral Devices, Inc. (2009), *RS³™ User Manual, ASD Doc. 600545 Rev. E*, Boulder, Colo. (Available at http://support.asdi.com/Document/Viewer.aspx?id=46.)

Babin, M., A. Morel, V. Fournier-Sicre, F. Fell, and D. Stramski (2003a), Light scattering properties of marine particles in coastal and open ocean waters as related to the particle mass concentration, *Limnol. Oceanogr.*, *48*(2), 843–859, doi:10.4319/lo.2003.48.2.0843.

Babin, M., D. Stramski, G. M. Ferrari, H. Claustre, A. Bricaud, G. Obolensky, and N. Hoepffner (2003b), Variations in the light absorption coefficients of phytoplankton, nonalgal particles, and dissolved organic matter in coastal waters around Europe, *J. Geophys. Res.*, *108*(C7), 3211, doi:10.1029/2001JC000882.

Barnard, A. H., J. R. V. Zaneveld, and W. S. Pegau (1999), In situ determination of the remotely sensed reflectance and the absorption coefficient: Closure and inversion, *Appl. Opt.*, *38*(24), 5108–5117, doi:10.1364/AO.38.005108.

Blough, N. V., O. C. Zafiriou, and J. Bonilla (1993), Optical absorption spectra of waters from the Orinoco River outflow: Terrestrial input of colored organic matter to the Caribbean, *J. Geophys. Res.*, *98*(C2), 2271–2278, doi:10.1029/92JC02763.

Brando, V. E., and A. G. Dekker (2003), Satellite hyperspectral remote sensing for estimating estuarine and coastal water quality, *IEEE Trans. Geosci. Remote Sens.*, *41*(6), 1378–1387, doi:10.1109/TGRS.2003.812907.

Bricaud, A., A. Morel, and L. Prieur (1981), Absorption by dissolved organic matter of the sea (yellow substance) in the UV and visible domains, *Limnol. Oceanogr.*, *26*(1), 43–53, doi:10.4319/lo.1981.26.1.0043.

Bricaud, A., A. Morel, M. Babin, K. Allali, and H. Claustre (1998), Variations of light absorption by suspended particles with chlorophyll *a* concentration in oceanic (case 1) waters: Analysis and implications for bio-optical models, *J. Geophys. Res.*, *103*(C13), 31,033–31,044, doi:10.1029/98JC02712.

Bukata, R. P., J. H. Jerome, A. S. Kondratyev, and D. V. Pozdnyakov (1995), *Optical Properties and Remote Sensing of Inland and Coastal Waters*, CRC Press, Boca Raton, Fla.

Carder, K. L., R. G. Steward, G. R. Harvey, and P. B. Ortner (1989), Marine humic and fulvic acids: Their effects on remote sensing of ocean chlorophyll, *Limnol. Oceanogr.*, *34*(1), 68–81, doi:10.4319/lo.1989.34.1.0068.

Carder, K. L., F. R. Chen, Z. P. Lee, S. K. Hawes, and D. Kamykowski (1999), Semianalytic Moderate-Resolution Imaging Spectrometer algorithms for chlorophyll *a* and absorption with bio-optical domains based on nitrate-depletion temperatures, *J. Geophys. Res.*, *104*(C3), 5403–5421, doi:10.1029/1998JC900082.

Carlson, C. A., H. W. Ducklow, and A. F. Michaels (1994), Annual flux of dissolved organic carbon from the euphotic zone in the northwestern Sargasso Sea, *Nature*, *371*, 405–408, doi:10.1038/371405a0.

Chang, G. C., and R. W. Gould (2006), Comparisons of optical properties of the coastal ocean derived from satellite ocean color and in situ measurements, *Opt. Express*, *14*(22), 10,149–10,163, doi:10.1364/OE.14.010149.

Chen, R. F. (1999), In situ fluorescence measurements in coastal waters, *Org. Geochem.*, *30*(6), 397–409, doi:10.1016/S0146-6380(99)00025-X.

Chen, R. F., and G. B. Gardner (2004), High-resolution measurements of chromophoric dissolved organic matter in the Mississippi and Atchafalaya River plume regions, *Mar. Chem.*, *89*(1–4), 103–125, doi:10.1016/j.marchem.2004.02.026.

Chen, R. F., P. Bissett, P. Coble, R. Conmy, G. B. Gardner, M. A. Moran, X. Wang, M. L. Wells, P. Whelan, and R. G. Zepp (2004), Chromophoric dissolved organic matter (CDOM) source characterization in the Louisiana Bight, *Mar. Chem.*, *89*(1–4), 257–272, doi:10.1016/j.marchem.2004.03.017.

Del Castillo, C. E., P. G. Coble, J. M. Morell, J. M. López, and J. E. Corredor (1999), Analysis of the optical properties of the Orinoco River plume by absorption and fluorescence spectroscopy, *Mar. Chem.*, *66*(1–2), 35–51, doi:10.1016/S0304-4203(99)00023-7.

Doerffer, R., and J. Fischer (1994), Concentrations of chlorophyll, suspended matter, and gelbstoff in case II waters derived from satellite coastal zone color scanner data with inverse modeling methods, *J. Geophys. Res.*, *99*(C4), 7457–7466, doi:10.1029/93JC02523.

Doerffer, R., and H. Schiller (1998), Determination of case 2 water constituents using radiative transfer simulation and its inversion by neural networks, in *Proceedings of Ocean Optics XIV* [CD-ROM], edited by S. G. Ackleson and J. Campbell, Off. of Nav. Res., Kailua-kona, Hawaii.

Doney, S. C., R. G. Najjar, and S. Stewart (1995), Photochemistry, mixing and diurnal cycles in the upper ocean, *J. Mar. Res.*, *53*(3), 341–369, doi:10.1357/0022240953213133.

D'Sa, E. J., R. L. Miller, and C. Del Castillo (2006), Bio-optical properties and ocean color algorithms for coastal waters influenced by the Mississippi River during a cold front, *Appl. Opt.*, *45*(28), 7410–7428, doi:10.1364/AO.45.007410.

Ferrari, G. M., M. D. Dowell, S. Grossi, and C. Targa (1996), Relationship between the optical properties of chromophoric dissolved organic matter and total concentration of dissolved organic carbon in the southern Baltic Sea region, *Mar. Chem.*, *55*(3–4), 299–316, doi:10.1016/S0304-4203(96)00061-8.

Fischer, J. (1985), On the information content of multispectral radiance measurements over an ocean, *Int. J. Remote Sens.*, *6*(5), 773–786, doi:10.1080/01431168508948498.

Gardner, G. B., R. F. Chen, and A. Berry (2005), High-resolution measurements of chromophoric dissolved organic matter (CDOM) in the Neponset River Estuary, Boston Harbor, MA, *Mar. Chem.*, *96*(1–2), 137–154, doi:10.1016/j.marchem.2004.12.006.

Garver, S. A., and D. A. Siegel (1997), Inherent optical property inversion of ocean color spectra and its biogeochemical interpretation: 1. Time series from the Sargasso Sea, *J. Geophys. Res.*, *102*(C8), 18,607–18,625, doi:10.1029/96JC03243.

Gordon, H. R., and A. Morel (1983), *Remote Assessment of Ocean Color for Interpretation of Satellite Visible Imagery: A Review*, Springer, New York.

Green, S. A., and N. V. Blough (1994), Optical absorption and fluorescence properties of chromophoric dissolved organic matter in natural waters, *Limnol. Oceanogr.*, *39*(8), 1903–1916, doi:10.4319/lo.1994.39.8.1903.

Green, R. E., R. W. Gould Jr., and D. S. Ko (2008), Statistical models for sediment/detritus and dissolved absorption coefficients in coastal waters of the northern Gulf of Mexico, *Cont. Shelf Res.*, *28*(10–11), 1273–1285, doi:10.1016/j.csr.2008.02.019.

Hochman, H. T., R. E. Müller-Karger, and J. J. Walsh (1994), Interpretation of the coastal zone color scanner signature of the Orinoco River plume, *J. Geophys. Res.*, *99*(C4), 7443–7455, doi:10.1029/93JC02152.

Hoge, F. E., and P. E. Lyon (1996), Satellite retrieval of inherent optical properties by linear matrix inversion of oceanic radiance models: An analysis of model and radiance measurement errors, *J. Geophys. Res.*, *101*(C7), 16,631–16,648, doi:10.1029/96JC01414.

Hoge, F. E., M. E. Williams, R. N. Swift, J. K. Yungel, and A. Vodacek (1995), Satellite retrieval of the absorption coefficient of chromophoric dissolved organic matter in continental margins, *J. Geophys. Res.*, *100*(C12), 24,847–24,854, doi:10.1029/95JC02561.

Huang, W., and R. F. Chen (2009), Sources and transformations of chromophoric dissolved organic matter in the Neponset River Watershed, *J. Geophys. Res.*, *114*, G00F05, doi:10.1029/2009JG000976.

Jerlov, N. G. (1976), *Marine Optics*, 2nd ed., Elsevier, Amsterdam.

Kirk, J. T. O. (1994), *Light and Photosynthesis in Aquatic Ecosystems*, 2nd ed., xvi + 509 pp., Cambridge Univ. Press, Cambridge, U. K.

Kowalczuk, P., J. Olszewski, M. Darecki, and S. Kaczmarek (2005a), Empirical relationships between coloured dissolved organic matter (CDOM) absorption and apparent optical properties in Baltic Sea waters, *Int. J. Remote Sens.*, *26*(2), 345–370, doi:10.1080/01431160410001720270.

Kowalczuk, P., J. Stoń-Egiert, W. J. Cooper, R. F. Whitehead, and M. J. Durako (2005b), Characterization of chromophoric dissolved organic matter (CDOM) in the Baltic Sea by excitation emission matrix fluorescence spectroscopy, *Mar. Chem.*, *96*(3–4), 273–292, doi:10.1016/j.marchem.2005.03.002.

Kratzer, S., D. Bowers, and P. B. Tett (2000), Seasonal changes in colour ratios and optically active constituents in the optical Case-2 waters of the Menai Strait, North Wales, *Int. J. Remote Sens.*, *21*(11), 2225–2246, doi:10.1080/01431160050029530.

Lane, R. R., J. W. Day, B. Marx, E. Reves, and G. P. Kemp (2002), Seasonal and spatial water quality changes in the outflow plume of the Atchafalaya River, Louisiana, USA, *Estuaries*, *25*(1), 30–42, doi:10.1007/BF02696047.

Lee, Z. (1994), Visible-infrared remote-sensing model and applications for ocean waters, Ph.D. thesis, 164 pp., Univ. of South Fla., St. Petersburg.

Lee, Z.-P. (Ed.) (2006), *Remote Sensing of Inherent Optical Properties: Fundamentals, Tests of Algorithms, and Applications*, *IOCCG Rep. 5*, Int. Ocean-Colour Coord. Group, Dartmouth, Nova Scotia, Canada.

Lee, Z. P., and K. L. Carder (2004), Absorption spectrum of phytoplankton pigments derived from hyperspectral remote-sensing reflectance, *Remote Sens. Environ.*, *89*(3), 361–368, doi:10.1016/j.rse.2003.10.013.

Lee, Z. P., K. L. Carder, T. G. Peacock, C. O. Davis, and J. L. Mueller (1996), Method to derive ocean absorption coefficients from remote-sensing reflectance, *Appl. Opt.*, *35*(3), 453–462, doi:10.1364/AO.35.000453.

Lee, Z. P., K. L. Carder, R. G. Steward, T. G. Peacock, C. O. Davis, and J. S. Patch (1998), An empirical algorithm for light absorption by ocean water based on color, *J. Geophys. Res.*, *103*(C12), 27,967–27,978, doi:10.1029/98JC01946.

Lee, Z., K. L. Carder, C. D. Mobley, R. G. Steward, and J. S. Patch (1999), Hyperspectral remote sensing for shallow waters: 2. Deriving bottom depths and water properties by optimization, *Appl. Opt.*, *38*(18), 3831–3843, doi:10.1364/AO.38.003831.

Lee, Z., K. L. Carder, R. F. Chen, and T. G. Peacock (2001), Properties of the water column and bottom derived from Airborne Visible Infrared Imaging Spectrometer (AVIRIS) data, *J. Geophys. Res.*, *106*(C6), 11,639–11,651, doi:10.1029/2000JC000554.

Lee, Z. P., K. L. Carder, and R. A. Arnone (2002), Deriving inherent optical properties from water color: A multiband quasi-analytical algorithm for optically deep waters, *Appl. Opt.*, *41*(27), 5755–5772, doi:10.1364/AO.41.005755.

Lee, Z. P., A. Weidemann, J. Kindle, R. Arnone, K. L. Carder, and C. Davis (2007), Euphotic zone depth: Its derivation and implication to ocean-color remote sensing, *J. Geophys. Res.*, *112*, C03009, doi:10.1029/2006JC003802.

Liu, C.-C., and R. L. Miller (2008), Spectrum matching method for estimating the chlorophyll-*a* concentration, CDOM ratio, and backscatter fraction from remote sensing of ocean color, *Can. J. Rem. Sens.*, *34*(4), 343–355.

Mannino, A., M. E. Russ, and S. B. Hooker (2008), Algorithm development and validation for satellite-derived distributions of DOC and CDOM in the U.S. Middle Atlantic Bight, *J. Geophys. Res.*, *113*, C07051, doi:10.1029/2007JC004493.

Maritorena, S., A. Morel, and B. Gentili (2000), Determination of the fluorescence quantum yield by oceanic phytoplankton in their natural habitat, *Appl. Opt.*, *39*(36), 6725–6737, doi:10.1364/AO.39.006725.

Mobley, C. D. (1994), *Light and Water: Radiative Transfer in Natural Water*, Academic, San Diego, Calif.

Mobley, C. D. (1999), Estimation of the remote-sensing reflectance from above-surface measurements, *Appl. Opt.*, *38*(36), 7442–7455, doi:10.1364/AO.38.007442.

Mobley, C. D., and L. K. Sundman (2008), *HydroLight 5, EcoLight 5: Technical Documentation*, Sequoia Sci., Inc., Bellevue, Wash.

Morel, A., and L. Prieur (1977), Analysis of variations in ocean color, *Limnol. Oceanogr.*, *22*(4), 709–722, doi:10.4319/lo.1977.22.4.0709.

Mueller, J. L., G. S. Fargion, and C. R. McClain (Eds.) (2003), *Biogeochemical and Bio-Optical Measurements and Data Analysis Methods*, *NASA Tech. Memo., NASA TM-2003-211621*, rev. 4, vol. 2.

Nelson, N. B., and D. A. Siegel (2002), Chromophoric DOM in the open ocean, in *Biogeochemistry of Marine Dissolved Organic Matter*, edited by D. A. Hansell and C. A. Carlson, pp. 547–578, Academic, Amsterdam.

Nelson, N. B., D. A. Siegel, and A. F. Michaels (1998), Seasonal dynamics of colored dissolved material in the Sargasso Sea, *Deep Sea Res., Part I*, *45*(6), 931–957, doi:10.1016/S0967-0637(97)00106-4.

O'Reilly, J. E., S. Maritorena, B. G. Mitchell, D. A. Siegel, K. L. Carder, S. A. Garver, M. Kahru, and C. McClain (1998), Ocean color chlorophyll algorithms for SeaWiFS, *J. Geophys. Res.*, *103*(C11), 24,937–24,953, doi:10.1029/98JC02160.

Pakulski, J. D., R. Benner, T. Whitledge, R. Amon, B. Eadie, L. Cifuentes, J. Ammerman, and D. Stockwell (2000), Microbial metabolism and nutrient cycling in the Mississippi and Atchafalaya River plumes, *Estuarine Coastal Shelf Sci.*, *50*(2), 173–184, doi:10.1006/ecss.1999.0561.

Prieur, L., and S. Sathyendranath (1981), An optical classification of coastal and oceanic waters based on the specific spectral absorption curves of phytoplankton pigments, dissolved organic matter, and other particulate materials, *Limnol. Oceanogr.*, *26*(4), 671–689, doi:10.4319/lo.1981.26.4.0671.

Qin, Y., V. E. Brando, A. G. Dekker, and D. Blondeau-Patissier (2007), Validity of SeaDAS water constituents retrieval algorithms in Australian tropical coastal waters, *Geophys. Res. Lett.*, *34*, L21603, doi:10.1029/2007GL030599.

Roesler, C. S., M. J. Perry, and K. L. Carder (1989), Modeling in situ phytoplankton absorption from total absorption spectra in productive inland marine waters, *Limnol. Oceanogr.*, *34*(8), 1510–1523, doi:10.4319/lo.1989.34.8.1510.

Sandidge, J. C., and R. J. Holyer (1998), Coastal bathymetry from hyperspectral observations of water radiance, *Remote Sens. Environ.*, *65*(3), 341–352, doi:10.1016/S0034-4257(98)00043-1.

Sathyendranath, S. (Ed.) (2000), *Remote Sensing of Ocean Colour in Coastal, and Other Optically-Complex, Waters*, *IOCCG Rep. 3*, Int. Ocean-Colour Coord. Group, Dartmouth, Nova Scotia, Canada.

Sathyendranath, S., F. E. Hoge, T. Platt, and R. N. Swift (1994), Detection of phytoplankton pigments from ocean color: Improved algorithms, *Appl. Opt.*, *33*(6), 1081–1089, doi:10.1364/AO.33.001081.

Sathyendranath, S., G. Cota, V. Stuart, H. Maass, and T. Platt (2001), Remote sensing of phytoplankton pigments: A comparison of empirical and theoretical approaches, *Int. J. Remote Sens.*, *22*(2–3), 249–273, doi:10.1080/014311601449925.

Shooter, D., and P. Brimblecombe (1989), Dimethylsulfide oxidation in the ocean, *Deep Sea Res., Part A*, *36*(4), 577–585, doi:10.1016/0198-0149(89)90007-1.

Siegel, D. A., and A. F. Michaels (1996), Quantification of non-algal light attenuation in the Sargasso Sea: Implications for biogeochemistry and remote sensing, *Deep Sea Res., Part II*, *43*(2–3), 321–345, doi:10.1016/0967-0645(96)00088-4.

Siegel, D. A., S. Maritorena, N. B. Nelson, D. A. Hansell, and M. Lorenzi-Kayser (2002), Global distribution and dynamics of colored dissolved and detrital organic materials, *J. Geophys. Res.*, *107*(C12), 3228, doi:10.1029/2001JC000965.

Stedmon, C. A., S. Markager, M. Søndergaard, T. Vang, A. Laubel, N. H. Borch, and A. Windelin (2006), Dissolved organic matter (DOM) export to a temperate estuary: Seasonal variations and implications of land use, *Estuaries Coasts*, *29*(3), 388–400, doi:10.1007/BF02784988.

U.S. Army Corps of Engineers (2008), The Atchafalaya Basin Project, report, New Orleans, La. (Available at http://www.mvn.usace.army.mil/pao/bro/AtchafalayaBasinProject.pdf.)

Valentine, R. L., and R. G. Zepp (1993), Formation of carbon monoxide from the photodegradation of terrestrial dissolved organic carbon in natural waters, *Environ. Sci. Technol.*, *27*(2), 409–412, doi:10.1021/es00039a023.

Van Der Woerd, H. J., and R. Pasterkamp (2008), HYDROPT: A fast and flexible method to retrieve chlorophyll-a from multispectral satellite observations of optically complex coastal waters, *Remote Sens. Environ.*, *112*(4), 1795–1807, doi:10.1016/j.rse.2007.09.001.

Vodacek, A., N. V. Blough, M. D. DeGrandpre, E. T. Peltzer, and R. K. Nelson (1997), Seasonal variation of CDOM and DOC in the Middle Atlantic Bight: Terrestrial inputs and photooxidation, *Limnol. Oceanogr.*, *42*(4), 674–686, doi:10.4319/lo.1997.42.4.0674.

Yentsch, C. S. (1962), Measurement of visible light absorption by particulate matter in the ocean, *Limnol. Oceanogr.*, *7*(2), 207–217, doi:10.4319/lo.1962.7.2.0207.

Yu, Q., Y. Q. Tian, R. F. Chen, A. Liu, G. B. Gardner, and W. N. Zhu (2010), Functional linear analysis for estimating riverine CDOM in coastal environment using in situ hyperspectral data, *Photogramm. Eng. Remote Sens.*, *76*(10), 1147–1158.

Zhan, H., S. Ping, and C. Chen (2005), A Bayesian based quasi-analytical algorithm for retrieval of inherent optical properties from ocean color, *Chin. Sci. Bull.*, *50*(23), 2770–2777, doi:10.1360/982004-828.

R. F. Chen, G. B. Gardner, and Y. Q. Tian, Department of Environmental, Earth and Ocean Sciences, University of Massachusetts Boston, 100 Morrissey Blvd., Boston, MA 02125, USA.

Q. Yu and W. Zhu, Department of Geosciences, University of Massachusetts Amherst, 611 N. Pleasant St., Amherst, MA 01003, USA. (qyu@geo.umass.edu)